GLOBAL BIOGEOCHEMICAL CYCLES, VOL. 14, NO. 1, PAGES 499-523, MARCH 2000

An eddy-permitting coupled physical-biological model of the North Atlantic
2. Ecosystem dynamics and comparison with satellite and JGOFS local studies data

Andreas Oschlies and Wolfgang Koeve,[1]

Institut für Meereskunde an der Universität Kiel, Kiel, Germany

Veronique Garçon

Laboratoire d'Etudes en Géophysique et Océanographie Spatiales, CNRS, UMR5566, Toulouse, France

Abstract. A model of biological production in the euphotic zone of the North Atlantic has been developed by coupling a Nitrate, Phytoplankton, Zooplankton, Detritus (NPZD) nitrogen-based ecosystem model with an eddy-permitting circulation model. The upper ocean physical and biological results are presented for an experiment with monthly climatological forcing. A comparison with satellite ocean color data shows that the model is capable of a realistic description of the main seasonal and regional patterns of surface chlorophyll. Agreement is also good for primary production except in the subtropical gyre where the model produces values more than an order of magnitude smaller than derived from satellite observations. In situ data available at Joint Global Ocean Flux Study (JGOFS) time series and local study sites (Bermuda Atlantic Time-series Study (BATS), 32°N, 65°W; North Atlantic Bloom Experiment (NABE), 47°N, 20°W; EUMELI oligotrophic, 21°N, 31°W) are used for a more detailed analysis of the model's capability to simultaneously reproduce seasonal ecosystem dynamics in different biological provinces of the North Atlantic Ocean. The seasonal cycle of phytoplankton biomass and nitrate is simulated quite realistically at all sites. Main discrepancies between model and observations are a large zooplankton peak, required by the model to end the phytoplankton spring bloom at the 47°N, 20°W site, and the underestimation of primary production at EUMELI and under oligotrophic summer conditions at BATS. The former model deficiency can be related to the neglect of phytoplankton aggregation; the latter is caused by too inefficient recycling of nutrients within the euphotic zone. Model improvements are suggested for further steps toward a realistic basin-wide multiprovinces simulation with a single ecosystem model.

1. Introduction

A realistic qualitative and quantitative description of pelagic ecosystem dynamics is a fundamental requirement for a comprehensive understanding of biogeochemical processes in the sea and their implications for the ocean's role in the global climate system. Intense observational programs like the Joint Global Ocean Flux Study (JGOFS) have successfully spent a lot of effort to improve our knowledge about ocean biogeochemistry. The emphasis of the observational program of JGOFS has been mainly on process studies (e.g., the North Atlantic Bloom Experiment (NABE) [*Ducklow and Harris*, 1993]) and time series studies (e.g., the Bermuda Atlantic Time-series Study (BATS) [*Michaels and Knap*, 1996]), which both, inherently, can only give a local view of the global ocean. Only satellite-based ocean color sensors, such as the Sea-viewing Wide Field-of-view Sensor (SeaWiFS), can provide synoptic observations of biological processes on a global scale. These observations are, however, restricted to the upper few meters of the water column, and their correct interpre-

[1]Also at the Institut für Ostseeforschung Warnemünde, Rostock, Germany.

Paper number 1999GB900080.
0886-6236/00/1999GB900080$12.00

tation depends on our knowledge of what is going on in the ocean interior.

It is hoped that numerical models can be used to interpolate between observations of different biological quantities at different times and different locations in a way that a dynamically consistent picture emerges. The development of such models always is a compromise between complexity, required to accurately reproduce detailed local measurements, and conceptual simplicity required for global applications and interpretations. A practical constraint is the finite memory of the computer that imposes limits on the number of explicitly resolved ecosystem variables. This is particularly important if high-resolution state-of-the art ocean circulation models are used to give an as realistic as possible description of the physical environment.

In a companion paper [*Oschlies and Garçon*, 1999] (hereafter referred to as OG99) we presented a simple four-compartment, nitrogen-based Nitrate, Phytoplankton, Zooplankton, Detritus (NPZD) pelagic ecosystem model coupled to an eddy-permitting circulation model of the North Atlantic. The sensitivity of the simulated upper ocean nitrate supply as well as of primary production was investigated with respect to the numerical realization of advection and the parameterization of turbulent mixing. It was found that the implicit numerical diffusivity inherent in standard upstream differencing could be orders of magnitudes larger than physically justified vertical diffusivities, particularly in the equatorial upwelling region. The resulting overestimation of vertical nutrient supply could be cured by switching to a second-order positive-definite advection scheme. An accurate description of vertical mixing was concluded to be of primary importance to control the simulated nutrient supply into the subtropical euphotic zone, whereas differences in the parameterization of viscosity were shown to affect the equatorial current system and associated upwelling features. In the present paper, the ecosystem model results of the standard experiment (A) selected by OG99 will be analyzed in greater detail. One of the major advances of this experiment with respect to a first basin-wide coupled biological-physical model for the North Atlantic Ocean presented by *Sarmiento et al.* [1993], hereafter SAR93, and *Fasham et al.* [1993], herafter FAS93, is a more realistic description of the physical environment, including an explicit representation of mesoscale variability.

Since the model is run with climatological forcing, we use observations averaged over many years whenever possible. The seasonal cycle of surface chlorophyll concentrations will be compared on the basin scale with satellite surface chlorophyll measurements from the Coastal Zone Color Scanner (CZCS) mission. Satellite-derived estimates of primary production will be used for a basin-wide comparison with model results. A more detailed investigation of the simulated ecosystem dynamics will then follow at three time series and process study sites in the North Atlantic, using data mainly gathered during JGOFS. These sites are the Bermuda Atlantic Time-series Study (BATS), 32°N, 65°W; the North Atlantic Bloom Experiment (NABE), 47°N, 20°W site; and the EUMELI oligotrophic site (21°N, 31°W). These individual sites may be viewed as representatives of different ecological provinces, ranging from the trade wind region to the northern boundary of the westerlies domain as classified by *Longhurst* [1995]. Model deficiencies identified at the individual sites are investigated, and model improvements are suggested. The discussion section also addresses the question to what extent we can expect that a single set of biological parameters can be used to model pelagic ecosystems on a basin scale.

2. Description of the Coupled Model

2.1. Physical Model

The physical model is based on the Geophysical Fluid Dynamics Laboratory's (GFDL) Modular Ocean Model (MOM) [*Pacanowski et al.*, 1991] primitive-equation ocean circulation model. The present configuration is based on the Community Modeling Effort (CME) model [*Bryan and Holland*, 1989] and covers the Atlantic Ocean between 15°S and 65°N with a grid spacing of 1/3° in meridional and 2/5° in zonal directions. A refined vertical grid has been used, increasing the number of levels in the upper 150 m from four to eleven (Table 1 of OG99). The model is forced with monthly climatological data sets (see OG99).

Turbulent vertical diffusion in and below the surface mixed layer is modeled using the Turbulent Kinetic Energy (TKE) closure of *Gaspar et al.* [1990] in the three dimensional (3-D) implementation proposed by *Blanke and Delecluse* [1993]. It solves a prognostic equation for TKE, considering turbulence generation by wind, buoyancy fluxes, and shear, as well as dissipation and turbulent diffusion of TKE. Together with a diagnostic turbulent mixing length this yields vertical diffusivities and viscosities at every grid point and time step of the numerical model. As discussed by OG99, the lower limit for TKE has been tuned to closely match recent observations of diapycnal diffusion in the thermocline [*Ledwell et al.*, 1993].

Horizontal subgrid-scale diffusion and dissipation are parameterized by the highly scale-selective biharmonic operator with both friction and diffusion coefficients set to $A_h = 2.5 \times 10^{19}\,\mathrm{cm^4\,s^{-1}}$. This form is commonly used in high-resolution models and reflects the notion that mixing along (approximately horizontal) isopycnal surfaces occurs mainly through the action of eddies and thus is supposed to be explicitly resolved by the model. Note, however, that in the present 1/3° grid configura-

tion eddy scales are not well reproduced by the model north of about 30°N [*Stammer and Böning*, 1992].

To ensure positive tracer concentrations, advection of ecosystem variables is often modeled by the sign-preserving upstream scheme. Among the advection schemes presently available (see *Hecht et al.* [1998] for a recent discussion) this is computationally cheapest, but has the disadvantage of very large implicit diffusion. In OG99 we have shown that this leads to a considerable overestimation of nutrient fluxes into the euphotic zone, particularly in the equatorial upwelling region. In the present study we therefore use the higher-order, less-diffusive Multidimensional Positive Definite Central Differences (MPDCD) scheme of *Lafore et al.* [1998]. It is based on the standard central difference equations, but computes a flux limitation to satisfy a sufficient condition for positiveness (see OG99 for a detailed description).

2.2. Biological Model

The ecosystem model is a simple nitrogen-based Nitrate, Phytoplankton, Zooplankton, Detritus (NPZD) pelagic model (OG99). The evolution of any biological tracer in the coupled biological-physical model is governed by an advective-diffusive equation plus a source-minus-sink term that describes changes due to biological activity. For the individual biological tracers the source-minus-sink terms are given by

$$\mathrm{sms}(P) = \overline{J}(z,t,N)\,P - G(P)\,Z - \mu_P\,P \quad (1)$$

$$\mathrm{sms}(Z) = \gamma_1 G(P)\,Z - \gamma_2 Z - \mu_Z\,Z^2 \quad (2)$$

$$\mathrm{sms}(D) = (1-\gamma_1)G(P)\,Z + \mu_P\,P + \mu_Z\,Z^2 - \mu_D\,D - w_s\frac{\partial D}{\partial z} \quad (3)$$

$$\mathrm{sms}(N) = \mu_D\,D + \gamma_2 Z - \overline{J}(z,t,N)\,P \quad (4)$$

Following *Hurtt and Armstrong* [1996], the phytoplankton growth rate is taken to be the minimum of light- and nutrient-limited growth,

$$\overline{J}(z,t,N) = \min\left(\overline{J}(z,t), J_{\max}\frac{N}{k_1+N}\right) \quad (5)$$

where $\overline{J}(z,t)$ denotes the purely light-limited growth rate averaged over 24 hours, and $J_{\max}$ is the light-saturated growth. $\overline{J}(z,t)$ is computed using the analytical method of *Evans and Parslow* [1985] (see also OG99). For zooplankton grazing we use a Holling type III function [*Fasham*, 1995]:

$$G(P) = \frac{g\epsilon\,P^2}{g+\epsilon\,P^2} \quad (6)$$

The individual parameters of the ecosystem model are listed in Table 1. As common in such simple, few-component ecosystem models, grazing parameters are more typical of microzooplankton rather than mesozooplankton.

All four ecosystem compartments are transported passively by advection and diffusion. Only detritus has an additional sinking velocity (constantly $5\,\mathrm{m\,d^{-1}}$) that allows it to move relative to the water. Once detritus reaches the ocean bottom, it is assumed to be buried immediately in the sediment. Regarding the relatively slow sinking velocity and high remineralization rate, this assumption was thought to be not critical on the considered timescales of a few years. While appropriate for the open ocean, this approach leads to an unrealistically fast removal of nitrogen from the water column in shallow shelf areas. For this reason, the sediment formulation has been changed in subsequent simulations with the coupled biological-physical model insofar as sinking through the bottom of the deepest grid box is not any longer allowed, leaving all detritus in the lowest grid box subject to advection, diffusion, and remineralization. For the pelagic open-ocean results presented in this paper, the sediment–water interaction is unimportant.

2.3. Initialization

The physical model was initialized with a spun-up state of a 24-year integration [*Böning et al.*, 1996] of the original CME model. After inclusion of the additional surface levels and the TKE closure scheme, the physical model was integrated for 1 year to adjust the upper ocean. Then the biology was inserted, to be integrated in fully coupled mode with the evolving physical fields over a 3-year period. The initial nitrate concentration field was taken from the climatological data of *Conkright et al.* [1994]. For the initial concentrations of P, Z, and D we followed SAR93: initial P and Z concentrations were set to $0.14\,\mathrm{mmol\,N\,m^{-3}}$ and $0.014\,\mathrm{mmol\,N\,m^{-3}}$ at the surface, respectively, decreasing exponentially with a scale depth of 100 m. D was initialized with a small value ($10^{-4}\,\mathrm{mmol\,N\,m^{-3}}$) everywhere. No restoring was applied to the biological tracers at the closed boundaries. As shown by OG99, a relatively stable seasonal cycle is established already after about 1 year. Results are presented for the third coupled year.

3. Basin-Scale Ecosystem Dynamics

3.1. Seasonal Cycle of Surface Chlorophyll

Satellite ocean color measurements provide the unpreceeded possibility for basin-wide observations of pelagic biological activity and its variability in space and time. While the wealth of coming data from sensors such as SeaWiFS has for a long time been anticipated, the only ocean color data set that presently al-

Table 1. Parameters of the Ecosystem Model

Parameter	Symbol	Value	Units
	Phytoplankton (P) Coefficients		
Integration method for daily growth rate		EP85	
Initial slope of P-I curve	α	0.025	$d^{-1}/(W\,m^{-2})$
Photosynthetically active ratiation	PAR	0.43	
Light attenuation due to water	k_w	0.04	m^{-1}
Light attenuation by phytoplankton	k_c	0.03	$m^{-1}\,(mmol\,m^{-3})^{-1}$
Maximum growth rate parameters	a	0.6	day^{-1}
	b	1.066	
	c	1.0	$(°C)^{-1}$
Half-saturation constant for N uptake	K_1	0.5	$mmol\,m^{-3}$
Specific mortality rate	μ_P	0.03	day^{-1}
	Zooplankton (Z) Coefficients		
Assimilation efficiency	γ_1	0.75	
Maximum grazing rate	g	2.0	day^{-1}
Prey capture rate	ϵ	1.0	$(mmol\,m^{-3})^{-2}\,d^{-1}$
(Quadratic) mortality	μ_Z	0.20	$(mmol\,m^{-3})^{-1}\,d^{-1}$
Excretion	γ_2	0.03	day^{-1}
	Detrital (D) Coefficients		
Remineralization rate	μ_D	0.05	day^{-1}
Sinking velocity	w_s	5.0	$m\,d^{-1}$

EP85 is *Evans and Parslow* [1985].

lows the computation of a climatological annual cycle of surface cholorophyll concentrations stems from the Coastal Zone Color Scanner (CZCS) mission and covers the period 1978–1986 [*Esaias et al.*, 1986; *Feldman et al.*, 1989].

In the model all biogeochemical fluxes as well as standing stocks are computed in nitrogen units. Hence surface chlorophyll is not a prognostic variable but has to be diagnosed from the model state. A constant conversion ratio of 1.59 g chlorophyll per mol nitrogen was chosen that corresponds to a chlorophyll to carbon mass ratio of 1:50 and a C:N mole ratio of 6.625 used throughout the paper.

Figure 1 displays seasonal means of the simulated chlorophyll concentration averaged over the upper 23 m, that is, the top two layers of the numerical model. This is the same depth average as was used by SAR93. Owing to the presence of a mixed layer model, the upper two layers of our model are almost always well mixed and virtually represent surface concentrations. Corresponding seasonal maps of CZCS deduced surface chlorophyll values are displayed in Figure 2. Despite the relatively large estimated errors of the CZCS derived chlorophyll concentrations, some 35% [*Gordon et al.*, 1983] with even more substantial errors during autumn and winter north of approximately 40°N [*Yoder et al.*, 1993], we preferred the long term average provided by the CZCS data to the more accurate SeaWiFS data so far available for a single year only. Overall, there is good qualitative agreement between patterns of modeled and observed surface chlorophyll, but simulated chlorophyll concentrations are generally lower than those inferred from the CZCS data.

The dominant feature of the seasonal cycle of surface chlorophyll in the mid and high-latitude North Atlantic is the basin-wide occurrence of a spring bloom. In winter the model shows an approximately zonal ridge of elevated surface chlorophyll ($> 0.5\,mg\,Chl\,m^{-3}$) between 35°N and 45°N extending from the northwestern flank of the subtropical gyre to the European coast. Particularly in the western basin this is in contrast to the CZCS data that show midlatitude winter concentrations of only about $0.2\,mg\,Chl\,m^{-3}$. The model-data discrepancy in this region will be discussed further when investigating the BATS site (32°N, 65°W) in section 4. In spring the CZCS data show high chlorophyll concentrations ($>0.5\,mg\,Chl\,m^{-3}$) almost everywhere in the subpolar North Atlantic north of a northeastward sloping

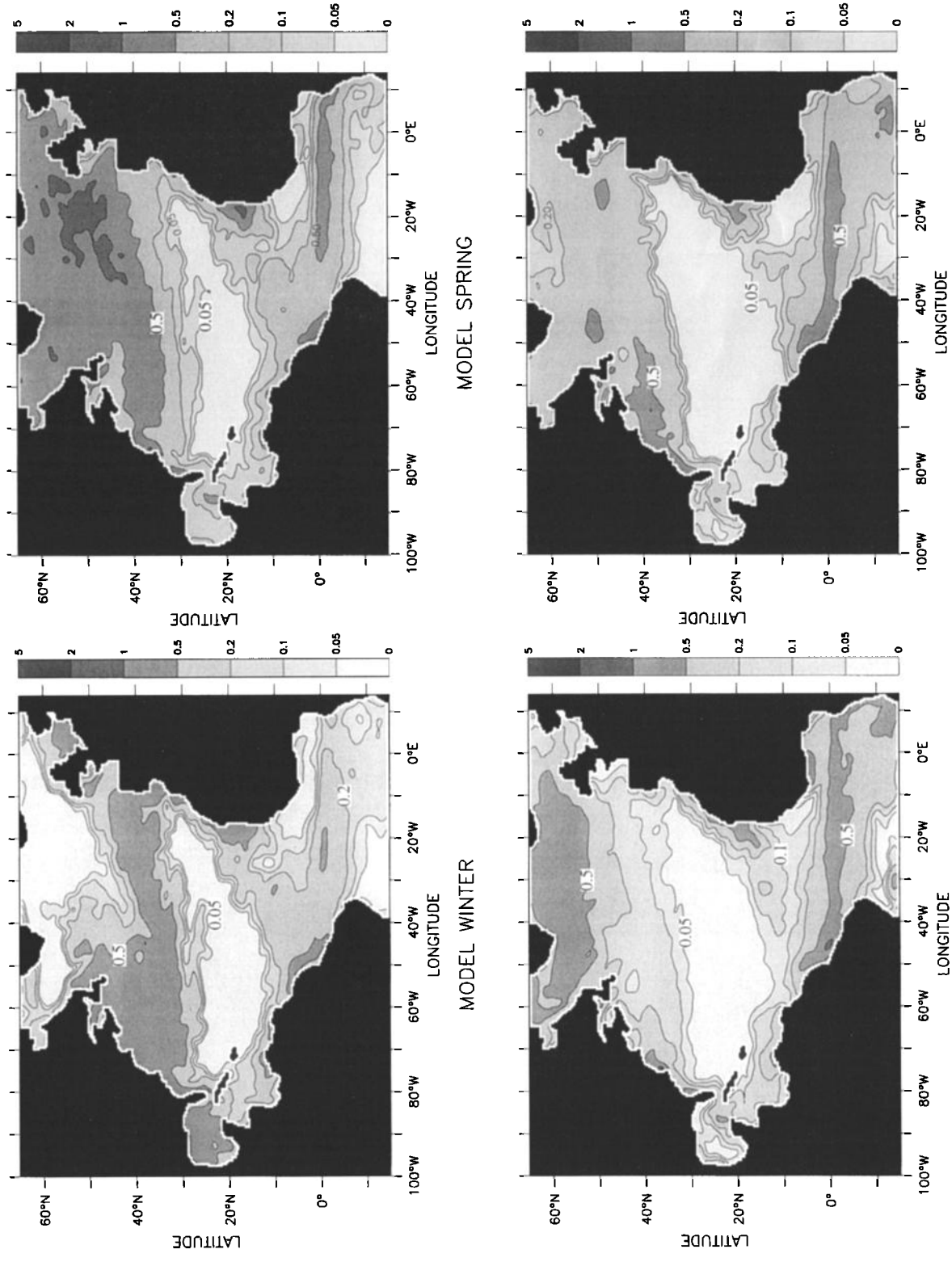

Figure 1. Seasonally averaged simulated surface chlorophyll in mg Chl m^{-3} computed from nitrogen via a constant ratio of 1 59 g chlorophyll per mol nitrogen Winter is defined as January through March

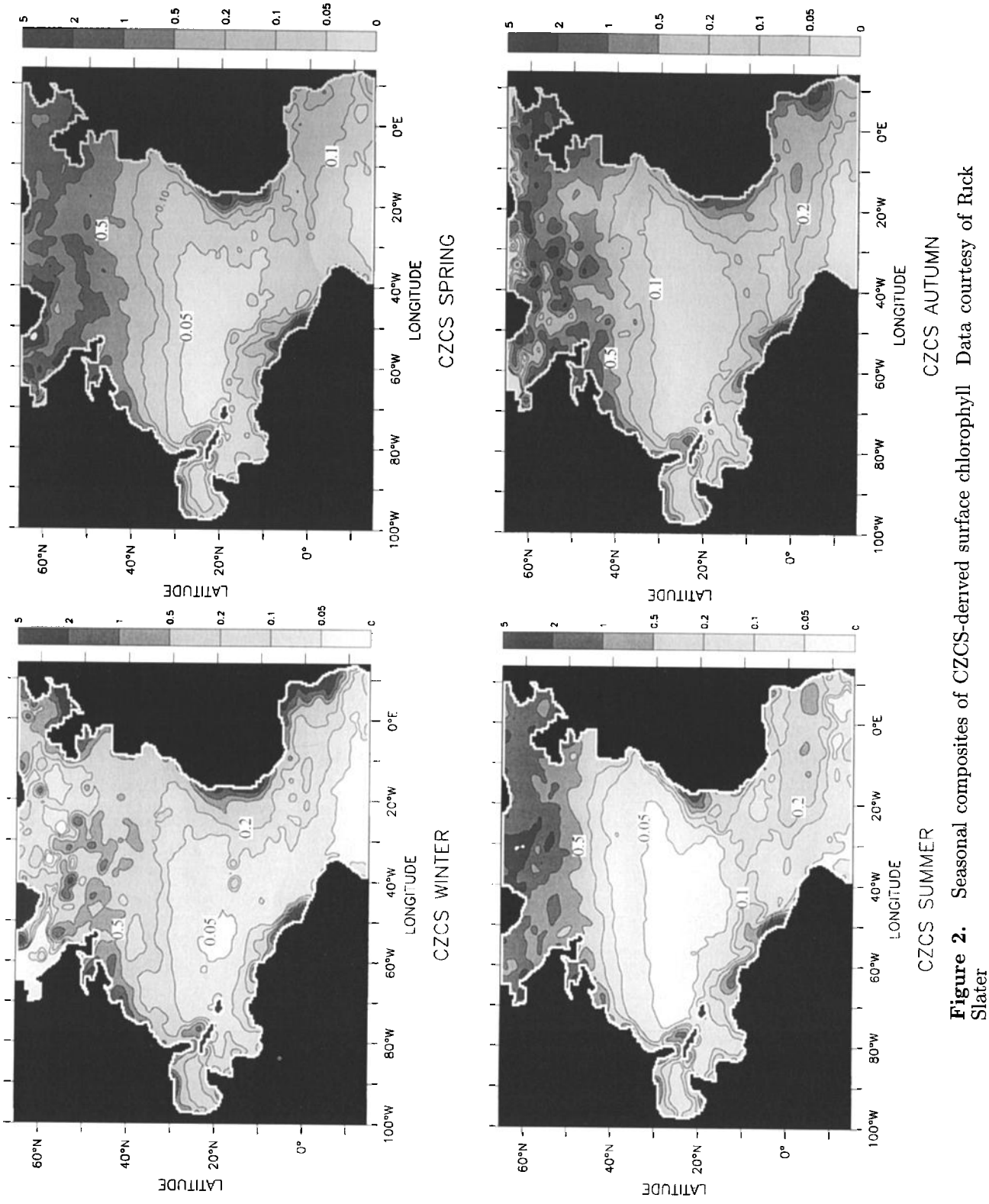

Figure 2. Seasonal composites of CZCS-derived surface chlorophyll Data courtesy of Rick Slater

line between 35°N on the American shelf to 45°N off Europe. This signal of the spring bloom is well reproduced by the model simulation, although simulated maximum concentrations (<2.0 mg Chl m^{-3} in the seasonal mean) are slightly lower and are situated farther south (~50°N) than in the CZCS data (>2.0 mg Chl m^{-3} at ~60°N). Summer chlorophyll concentrations stay high only north of about 50°N both in the observations and in the model, but again, simulated concentrations do not reach the satellite estimates.

The interior of the oligotrophic subtropical gyre is characterized by low surface chlorophyll concentrations in both the CZCS data and the model results. Agreement between data and model is very close in spring and summer. However, the CZCS data show concentrations of up to 0.1 mg Chl m^{-3} in autumn and winter whereas simulated concentrations stay less than 0.05 mg Chl m^{-3} during all seasons. This is an indication that in the model the subtropical gyre is too oligotrophic. We will reiterate this subject in the following section as well in the discussion of the model results at the EUMELI site in section 4.

Good qualitative agreement is found in the patterns reflecting upwelling regions off West Africa and South America, although simulated chlorophyll concentrations are substantially lower than those derived from the CZCS data. As noted, for example, by *Sathyendranath and Morel* [1983], CZCS retrievals are particularly unreliable in coastal seas where high loads of dissolved organic matter may erroneously be interpreted as chlorophyll. While this is an important restriction of CZCS data on the continental shelf, it can not explain the model's underestimation farther offshore, for example, in the Gulf of Guinea, particularly in autumn and winter.

Simulated chlorophyll values systematically exceed the CZCS observations along the equator. In fact, our simulated concentrations are very similar to those obtained by SAR93 (their Figure 2), who attribute such high surface values to the overestimated equatorial upwelling in their model. As discussed by OG99, there is no evidence for too strong equatorial upwelling in the model used here. *Monger et al.* [1997] pointed out that climatological CZCS products may considerably underestimate chlorophyll concentrations in the eastern equatorial upwelling region. However, this would not explain model-data discrepancies in the central and western equatorial Atlantic. These may instead suggest deficiencies of the biological model like, for example, the neglect of dissolved organic matter (DOM). The inclusion of DOM has been proposed to remedy too high equatorial production in biogeochemical ocean models [e.g., *Six and Maier-Reimer*, 1996], although a recent study by *Aumont et al.* [1999] reported that the apparent need for DOM might have been related to model errors in the circulation field. For the present model the neglect of DOM may also explain overestimated equatorial nitrate concentrations reported by OG99 even when the higher-order MPDCD advection was used. As yet, it is not clear to what extent this is an artifact of the closed southern boundary of the model. Experiments with a different southern boundary condition are presently under way in order to investigate this issue.

A peculiar feature of the model results are the very low chlorophyll concentrations at both entrances of the English Channel. For computational reasons, Great Britain is not separated from the Continent in our model configuration. Hence both entries of the Channel are dead ends with greatly reduced water exchange. Moreover, the assumed instantaneous removal of any detrital matter that reaches the bottom (see section 2.2) is not realistic in this shallow region. Subsequent simulations which leave detritus available for remineralization after it has reached the bottom yield higher surface chlorophyll concentrations close to the English Channel that are similar to the concentrations in the adjacent open seas.

3.2. Annual Primary Production

Maps of annual primary production were one of the principal diagnostics used by OG99 to demonstrate the strong sensitivity of the coupled ecosystem-circulation model to apparently small changes in numerics and physics. While OG99 concentrated on relative differences between the individual simulations, here we will present a more quantitative investigation.

Figure 3a shows the simulated annual primary production. Values are highest in the upwelling region off West Africa, exceeding 200 g C m^{-2} yr^{-1}. Further local maxima are found along the equator, with values larger than 100 g C m^{-2} yr^{-1} off the South American coast, smaller rates in the western basin (50–100 g C m^{-2} yr^{-1}), and higher production (100–200 g C m^{-2} yr^{-1}) toward the eastern basin. For comparison, the data of *Antoine et al.* [1996], hereafter AAM96, and *Behrenfeld and Falkowski* [1997], hereafter BF97, are displayed in Figures 3b and 3c, respectively. Although derived from the same CZCS data, there is considerable disparity between both production estimates. As discussed by BF97, this can be explained to a large extent by different assumptions made about the effect of temperature on production rates. Note that both satellite-derived production estimates are systematically higher (by a factor of 2 or more) than, for example, *Berger*'s [1989] compilation of in situ measurements. Explanations that have been put forward to resolve this observational discrepancy include the possible underestimation of early, not trace-metal clean in situ measurements [*Fitzwater et al.*, 1982] as well as large uncertainties in procedures employed to derive productivity from satellite measurements of ocean color (AAM96).

In the tropics, simulated primary production reaches

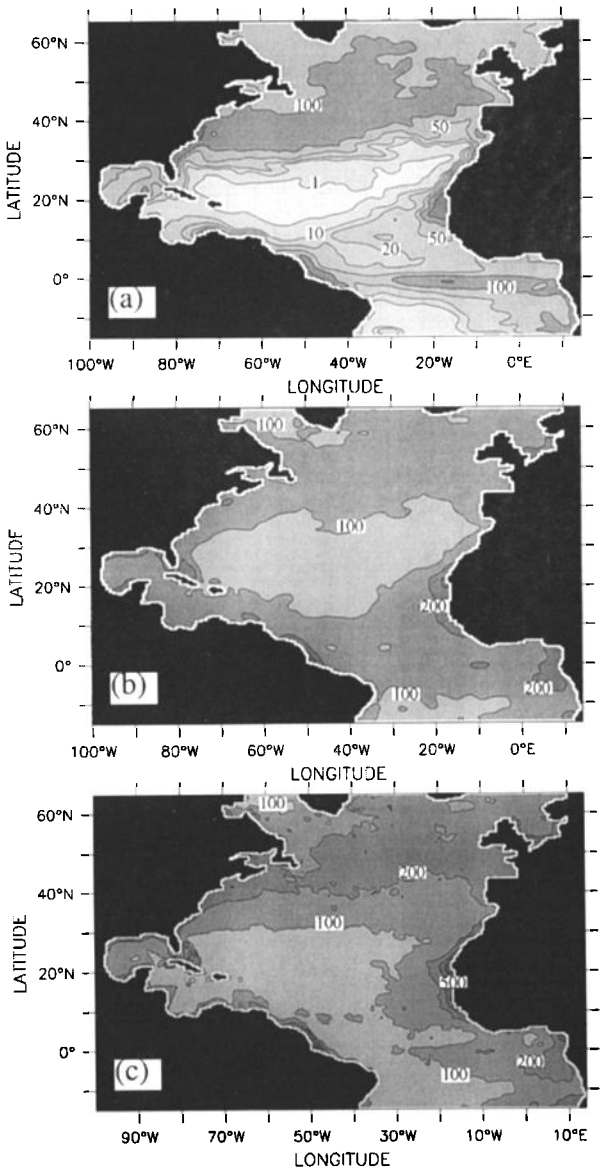

Figure 3. Annual primary production for (a) the model simulation, (b) the CZCS-data derived estimate by *Antoine et al.* [1996], and (c) the CZCS-data derived estimate by *Behrenfeld and Falkowski* [1997]. Contour lines are at 1, 10, 20, 50, 100, 200, 500, and 1000 g C m^{-2} yr^{-1}.

satellite-derived estimates only right at the equator. In contrast to the satellite data, the equatorial productivity maximum in the model is too pronounced (as is the chlorophyll maximum in Figure 1). Already a few degrees north and south of the equator, simulated production rates are systematically lower than found in either the AAM96 or the BF97 data.

The most alarming discrepancy between either observational estimate (including *Berger*'s [1989]) of primary production and our model results is apparent in the southern half of the subtropical gyre In this region, simulated primary production does not even reach 1 g C m^{-2} yr^{-1}, whereas both AAM96 as well as BF97 report values larger than 50 g C m^{-2} yr^{-1}. *Berger*'s [1989] map shows values between 25 and 35 g C m^{-2} yr^{-1} over large parts of the subtropical gyre, with only the very central regions exhibiting rates less than 25 g C m^{-2} yr^{-1}. Interestingly, the coarse-resolution model of SAR93 produced similarly low production rates as our eddy-permitting model.

It is known that in our model eddy energy is considerably underestimated [*Stammer and Böning*, 1992] This is a general problem of present state-of-the-art circulation models [e.g., *Stammer et al.*, 1996] and may be cured by even higher grid resolutions. For coupled ecosystem-circulation modeling, the underestimation of eddy activity is thought to be of particular concern in the subtropical ocean. In this region of steady Ekman downwelling (of about 50 m yr^{-1} [e.g., *McClain and Firestone*, 1993]), eddy pumping of nutrients into the euphotic zone has been proposed as an important mechanism for fueling biological production [e.g., *Jenkins*, 1988; *Dadou et al.*, 1996; *McGillicuddy et al.*, 1998]

Acknowledging that the too low biological production in the subtropical gyre may well be caused by the model's underestimation of eddy activity, we have also carried out an experiment with a considerably improved level of eddy activity in the model by assimilating satellite altimeter data from the simultaneous TOPEX/Poseidon and ERS-1 missions [*Oschlies and Garçon*, 1998]. Although this more realistic simulation of eddy variability resulted in an increase of subtropical primary production by about 60%, it still did not come close to observed levels in the central subtropical gyre *Oschlies and Garçon* [1998] put forward possible causes for this considerable underestimation of biological production in the subtropical gyre, including underestimation of rapid recycling within the euphotic zone, and the neglect of nitrogen fixation and lateral transport of DOM.

In midlatitudes, simulated annual primary production ranges from 100 to 200 g C m^{-2} yr^{-1}. Estimates of annual primary production based on satellite ocean color data vary from 100–200 g C m^{-2} yr^{-1} (Figure 3b, AAM96) to values exceeding 200 g C m^{-2} yr^{-1} (Figure 3c, BF97), whereas *Berger*'s [1989] compilation gives values of less than 100 g C m^{-2} yr^{-1}. Our simulated annual primary production in the midlatitude Atlantic thus falls well in between these estimates.

At higher latitudes, north of about 55°N, the model predicts a slight decrease in primary production to values less than 100 g C m^{-2} yr^{-1}. The maps of AAM96 and BF97 show such a decrease only for the Labrador Sea but not for the eastern basin, where the satellite-based estimates in general stay above 100 g C m^{-2} yr^{-1} south of 65°N As there is substantial doubt on the ac-

curacy of CZCS at high latitudes [*Yoder et al.*, 1993], we shall not overemphasize this discrepancy. Note, however, that *Berger's* [1989] compilation also shows a general northward increase of primary production up to about 65°N, reaching values between 90 and 125 g C m^{-2} yr^{-1}.

4. Annual Cycle at Selected JGOFS Time Series and Process Study Sites

In this section we investigate the model's seasonal cycle at three stations located in different biological provinces of the North Atlantic. The observational data base at these sites was obtained mainly during JGOFS and will be used to assess the quality of our simulation. Model deficiencies will be identified and routes for future improvement will be suggested.

We begin with the BATS site in the western subtropical gyre, before analyzing the model results at the NABE 47°N site in the North Atlantic drift province as defined by *Longhurst* [1995]. Finally, the results of an oligotrophic regime in the trade wind domain in the eastern subtropical gyre will be presented and compared with data taken during the EUMELI cruises.

Main integral quantities simulated by the model at the three sites are summarized in Table 2. Values shown include annual primary production, nitrate supply, and export of particulate organic nitrogen (PON) as well as their ratios which may be taken as approximation to the f ratio. Annual mean nitrogen fluxes between the ecosystem compartments are shown in Figure 4. All fluxes are integrated over the top 126 m of the model (i.e., the top 10 grid boxes) which was taken as proxy for the depth of the euphotic zone. In a 3-D z level model it is practical to use the same constant-depth criterion everywhere, although the depth of the euphotic zone will vary in space and time. The 126 m level can be regarded as its maximum depth. Because of shallow remineralization, the PON export across 126 m will in general be less than that leaving the euphotic zone. Similarly, lateral transport processes acting between the euphotic zone depth and the 126 m level may locally alter the nitrate supply.

All values shown are from the third year of the coupled model run. An integration over 2 more years did not show significant changes in mean properties. However, at the individual locations investigated here, physically driven fluctuations that appear naturally in the high-resolution model generate some year-to-year variations. Interannual variations in the values given in Table 2 and Figure 4 are generally small ($\sim$ 10%). A noteworthy exception is the nitrate input at the NABE 47°N site that is unusually low because of a large horizontal transport divergence (Table 2) in summer (see Figure 11 below) that is not present in other years. This flux divergence occurs well below the summer mixed layer and does not significantly affect the seasonally varying ecosystem dynamics discussed below. Both Table 2 and Figure 4 will be referred to repeatedly in the following subsections for the individual sites.

Table 2. Simulated Annual Nitrogen Fluxes at Three JGOFS Study Sites

	BATS	NABE	EUMELI
Primary Production	1.20	1.36	0.047
NO_3 input 0–126 m	0.64*	0.28	0.003
PON export† 0–126 m	0.69	0.47	0.015
NO_3 input/PP	0.53	0.21	0.06
PON export†/PP	0.57	0.35	0.32
NO_3 Transport Fluxes 0–126 m			
Vertical mixing	0.66	0.50	0.021
Vertical advection	-0.13	-0.09	-0.023
Horizontal transport	0.10	-0.13	0.005
Detritus Transport Fluxes 0–126 m			
Vertical mixing	0.03	0.01	0.000
Vertical adv. + sinking	-0.37	-0.41	-0.033
Horizontal transport	-0.01	-0.01	0.002
Total	-0.35	-0.41	-0.031
Phytoplankton Transport Fluxes 0–126 m			
Vertical mixing	-0.26	-0.05	-0.000
Vertical advection	-0.01	-0.00	0.000
Horizontal transport	0.00	0.01	0.012
Total	-0.27	-0.05	0.012
Zooplankton Transport Fluxes 0–126 m			
Vertical mixing	-0.06	-0.00	-0.000
Vertical advection	-0.01	0.00	0.000
Horizontal transport	-0.00	-0.01	0.003
Total	-0.07	-0.01	0.003

* *Oschlies and Garçon* [1998] reported 0.50 mol m^{-2} yr^{-1} for a 2°×2° running-mean average centered at BATS.
† "PON export" is vertical plus horizontal export of Phytoplankton + Zooplankton + Detritus.
Units are mol N m^{-2} yr^{-1}; positive values refer to input into the upper 126 m (except for PON export). Numbers are for the third coupled year.

4.1. Bermuda Atlantic Time Series Study

Following oceanographic and biogeochemical time series programs (in particular, Hydrostation S) close to Bermuda, BATS has been set up at about 32°N, 65°W by the U.S. JGOFS in October 1988. Since then, a wide range of biogeochemical parameters have been measured at least once per month. A recent overview of the database is given by *Michaels and Knap* [1996].

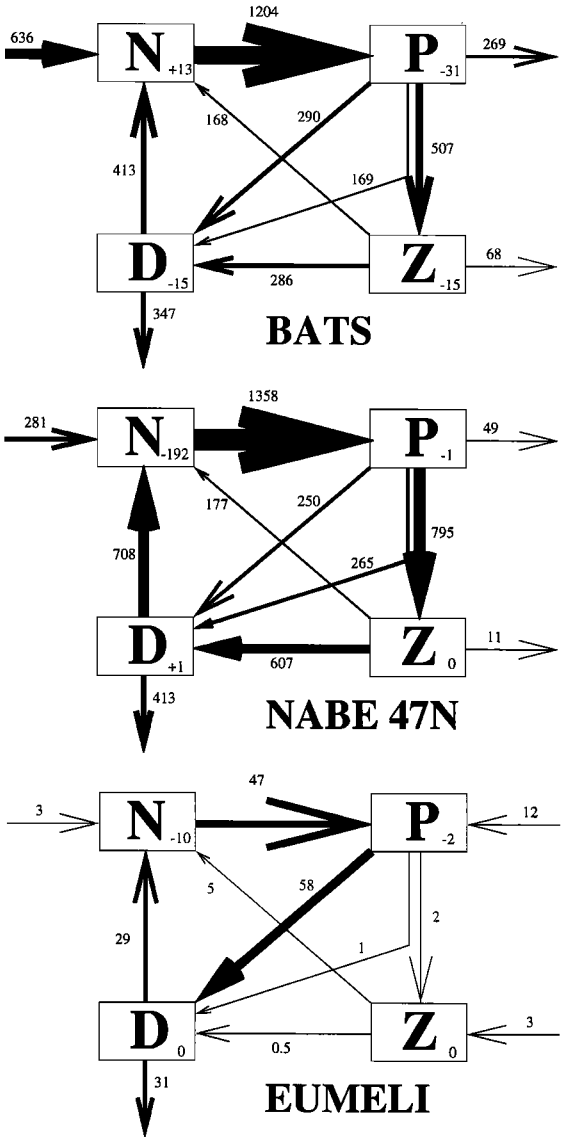

Figure 4. Annual fluxes of nitrogen between the compartments of the NPZD ecosystem model at (top) BATS, (middle) NABE 47°N, and (bottom) the EUMELI oligotrophic site. Fluxes are integrated over the upper 126 m, units are mmol N m^{-2} yr^{-1}. The thickness of the arrows is proportional to the magnitude of the flux; arrows for EUMELI are 10 times thicker than those for BATS and NABE 47°N. Arrows connected only to a single compartment refer to physically induced input/export of matter and to sinking of detritus. Numbers in the compartment boxes denote changes in stock size between beginning and end of year 3 of the coupled simulation. Such local imbalances are mainly an artifact of internal (e.g., mesoscale) variability in the physical model.

BATS is situated near the northwestern edge of the North Atlantic subtropical gyre in a region of weak Gulf Stream recirculation with a mean flow toward the southwest [*Siegel and Deuser*, 1997]. Ekman convergence induces a mean downwelling in the upper ocean of about 30 m yr^{-1} [*McClain and Firestone*, 1993]. Mesoscale variability was observed and was suggested as an important vehicle to flux significant amounts of nutrients into the euphotic zone near Bermuda [*Jenkins*, 1988; *McGillicuddy et al.*, 1998]. *Oschlies and Garçon* [1998] demonstrated for the same model as used here that mesoscale variability accounts for about 30% of the simulated nitrate flux into the upper ocean in the BATS area.

The simulated annual primary production at BATS amounts to 1.2 mol N m^{-2} (95 g C m^{-2}), which is between the older observations (72 g C m^{-2} yr^{-1}) of *Menzel and Ryther* [1960] and the more recent BATS measurements (125 g C m^{-2} yr^{-1}) reported by *Lohrenz et al.* [1992]. The annual nitrate supply (0.64 mol m^{-2}) is in good agreement with *Jenkins'* [1988] long-term averaged estimate of upward nitrate flux (0.56±0.16 mol N m^{-2}). Observations with shallow traps at a depth of 150 m revealed PON fluxes of 0.11 mol m^{-2} yr^{-1} [*Lohrenz et al.*, 1992], and 0.33 mol m^{-2} yr^{-1} when downward mixing of suspended PON was taken into account [*Altabet*, 1989]. This is not sufficient to close the upper ocean nitrogen budget, and there has been some debate about the role of dissolved organic matter (DOM) [e.g., *Carlson et al.* 1994]. Note, however, that convective export of DOM has been demonstrated for carbon (DOC) only and that C:N ratios of DOM may be much larger than the standard Redfield ratio [*Kähler and Koeve*, 1999]. In the present model configuration, DOM is not included, hence all nitrogen export has to occur via particulate matter. Indeed, the simulated PON export on average balances the nitrate supply (Table 2 and Figure 4). Note the relatively high contribution of phytoplankton to the PON export. Since in the model only detritus sinks relative to the water, this indicates the important contribution (~50%) of export via turbulent mixing and detrainment out of the upper 126 m. This is consistent with the observations of *Altabet* [1989] and also with previous 1-D model studies of *Doney et al.* [1996].

4.1.1. Seasonal cycle of the mixed layer. The annual cycle of upper ocean temperature simulated by the climatologically forced model at the BATS site is shown in Figure 5 together with the climatological seasonal cycle computed from 8 years of BATS data (1989–1996). Included as dotted (dashed) lines are the depth levels at which temperature deviates by more than 0.1 (0.5) degrees Celsius from the sea surface temperature (SST). Simulated mixed layer temperatures vary between 19.5°C in winter and 27.4°C in summer, which agrees well with the climatological data. Obviously, winter mixed layers are deeper in the model simulation than in the 8-year average of BATS data, whereas in summer the mixed layer depth (MLD) is less than 20 m both in the model and in the climatology. Actual winter MLDs observed at BATS ($\Delta T = 0.5$°C) varied between

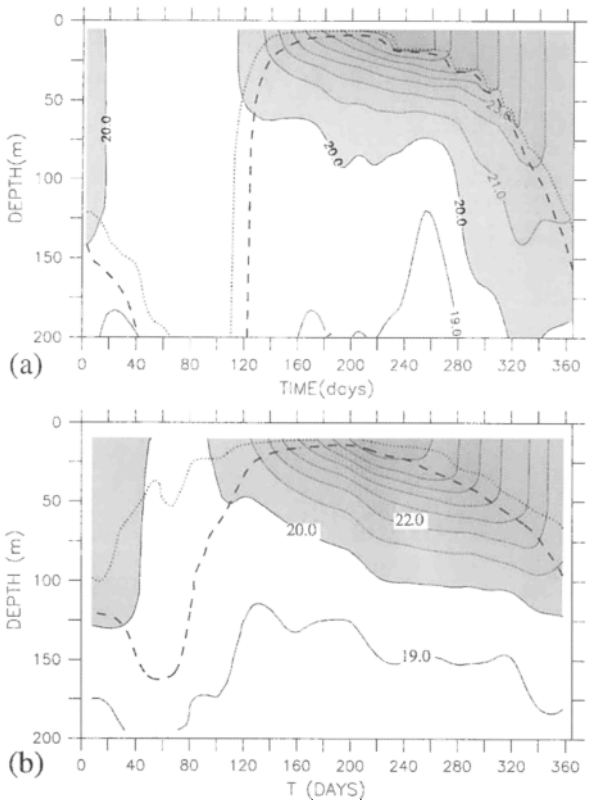

Figure 5. Annual cycle of temperature in the upper 200 m at the BATS site. (a) As simulated by the model; (b) as deduced from an objective analysis of the BATS data (obtained via `http://www.bbsr.edu`) for the 8-year period 1989 to 1996. Contour interval is 1°C, and the dotted and dashed lines indicate the depth where temperature deviates by 0.1°C and 0.5°C from the surface temperature.

150 m (in 1990) and 300 m (in 1994), with some deeper MLDs (> 400 m) present in the much longer time series at Hydrostation S during the 1960s [*Michaels and Knap*, 1996]. Since maximum depths occur at different times in different winters, they do not show up in the 8-years mean temperature field. The simulated MLD of 240 m (300 m) for the $\Delta T = 0.1$°C ($\Delta T = 0.5$°C) criterion is therefore well within the observational range.

4.1.2. Winter and spring. There is observational evidence that winter mixed layer generally penetrates the nitracline at the BATS site, giving rise to maximum surface nitrate values in winter and the subsequent development of a chlorophyll maximum [e.g., *Michaels and Knap*, 1996]. Since 1989, the BATS program found maximum winter nitrate concentrations of 0.3 mmol NO_3 m^{-3} in the surface mixed layer (Figure 6b). From correlations between temperature and nitrate *Michaels and Knap* [1996] estimated surface nitrate concentrations as high as 6 mmol m^{-3} in the late 1960s (when direct nitrate measurements were not available). Simulated nitrate concentrations reach maximum winter values of 1.4 mmol m^{-3} in the surface mixed layer (Figure 6a).

Figure 7 shows that the simulated mixed-layer averaged phytoplankton growth rates exceed the constant mortality of 0.03 d^{-1} (Table 1) during the period mid-November until mid-May (days 320–150). Despite the relatively deep mixed layers, there is still sufficient light to allow for net phytoplankton growth. Vertically integrated phytoplankton stocks as well as primary production and PON export show a net increase during winter (Figure 8). Modeled chlorophyll concentrations stay above 0.5 mg m^{-3}. The shallowing of the mixed layer around day 105 leads to an increase to maximum values of 1.2 mg m^{-3}, exceeding observed concentrations by about a factor 2 (Figure 9). The increase in phytoplankton biomass is followed by a rapid rise in zooplankton and detritus (Figure 8a). There are only very few zooplankton measurements at BATS. These indicate that integrated stocks of nanozooplankton and microzooplankton are always below 10 mmol N m^{-2} [*Roman et al.*, 1995], whereas the model reaches peak values about 5 times that high.

Vertically integrated primary production is shown in Figure 8b. Agreement with BATS data is gener-

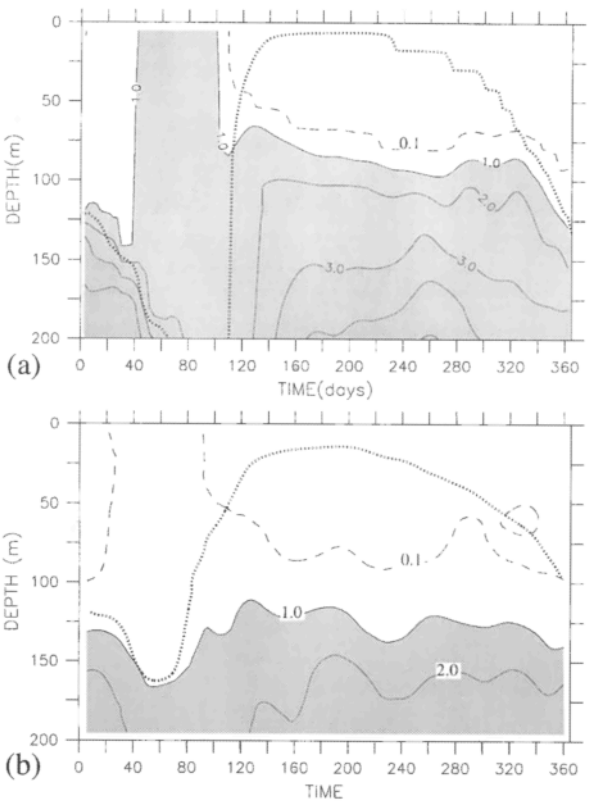

Figure 6. (a) Simulated and (b) observed annual cycle of nitrate at BATS (obtained via `http://www.bbsr.edu`). Observations are averaged over the years 1989 to 1996. Contour interval is 1 mmol m^{-3} with an additional dotted line at 0.1 mmol m^{-3}

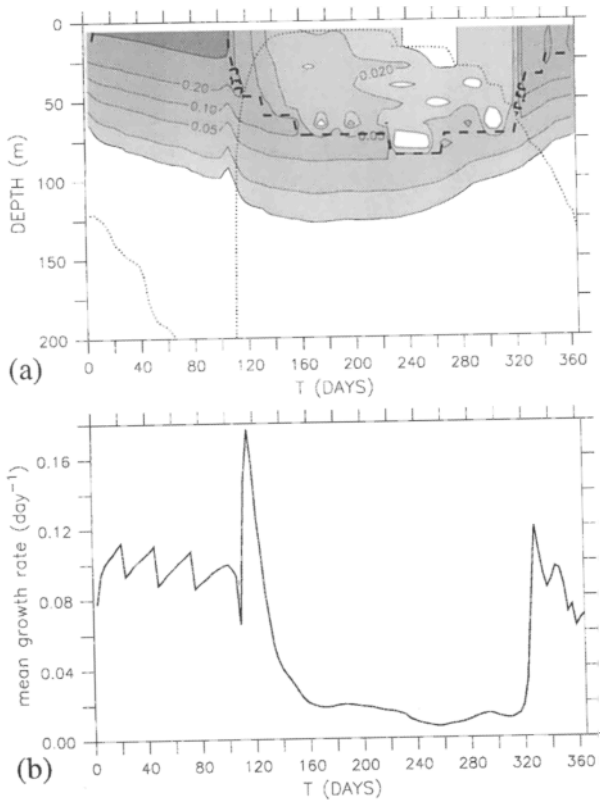

Figure 7. (a) Simulated phytoplankton growth rate at the BATS site. Isolines are at 0.01, 0.02, 0.05, 0.1, 0.2, and 0.5 day^{-1}. Regions above the heavy dashed line denote nutrient-limited growth, and elsewhere growth is light-limited. The dotted line refers to the bottom of the mixed layer defined by a $\Delta T = 0.1°C$ criterion. (b) Simulated phytoplankton growth averaged over the surface mixed layer indicated in Figure 7a.

ally good during winter and spring. Also included in Figure 8b is the export of detritus and of total PON. Consistent with the observations of *Altabet* [1989] turbulent downward transport of particles (particularly phytoplankton, see Table 2) is important. The distinct export maximum in spring found in shallow traps ($\sim$1 mmol N m^{-2} d^{-1} [e.g., *Michaels and Knap*, 1996]) is similar to the simulated flux of sinking detritus.

4.1.3. Summer and autumn. In summer and autumn, nitrate is exhausted both in the observations and in the model (Figure 6). A subsurface chlorophyll maximum develops at about 80 m that agrees well with the observations (Figure 9). While simulated phytoplankton stocks are within the observed range during summer (Figure 8a), vertically averaged primary production clearly is much too low in the model (Figure 8b). Within the nutrient-depleted mixed layer, primary production falls even below values of 0.1 mg C m^{-3} d^{-1}. This corresponds to the extremely low growth rates seen in Figure 7 In the absence of an explicitly modeled ammonium pool the present model formulation does not allow for growth in the absence of nitrate

Below the euphotic zone, simulated summer nitrate levels exceed observed concentrations (Figure 6) This may indicate a too shallow remineralization of detritus A side effect is an overestimated vertical gradient in the summer nitracline, which will tend to overestimate the, albeit small, diffusive fluxes of nitrate into the euphotic zone during summer.

4.1.4. Summary: BATS. Although annual mean values of both primary production and nitrate input are in reasonable agreement with observations, the simulated annual cycle shows considerable discrepancies primary production is much too low in summer, whereas biomass is overestimated in spring, possibly indicating a too strong flux of nitrate into the euphotic zone. These systematic errors in the simulated seasonal cycle are remarkedly robust under changes of the parameterization of vertical turbulent mixing (OG99) or of the level of

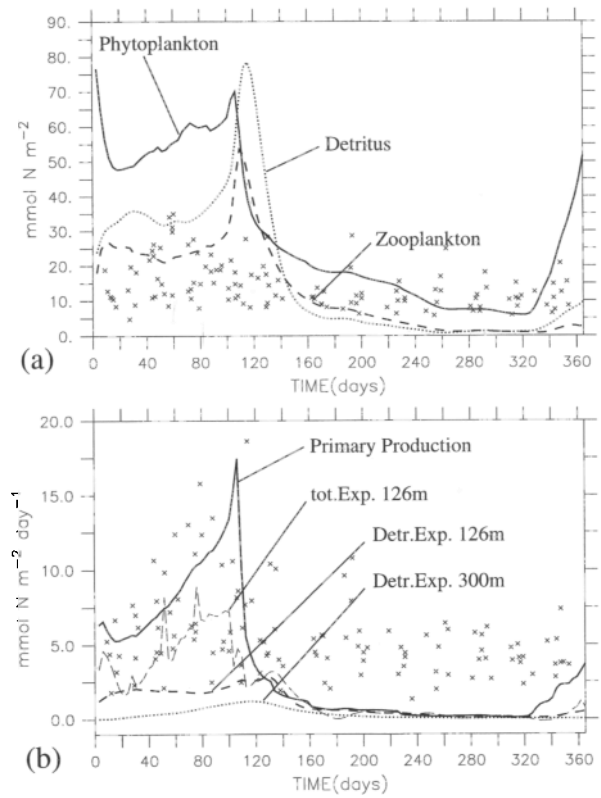

Figure 8. (a) Evolution of standing stocks of phytoplankton, zooplankton, and detritus at the BATS site, integrated over the top 150 m. Crosses represent observations taken during 1989-1996, converted to nitrogen using 1.59 g Chl per mol nitrogen. (b) Annual cycle of primary production (integrated over the upper 300 m) and PON export out of the upper 150 m and 300 m, respectively. Crosses refer to the BATS primary production measurements during 1989-1996 which were converted from carbon to nitrogen by a standard Redfield ratio of 6.625

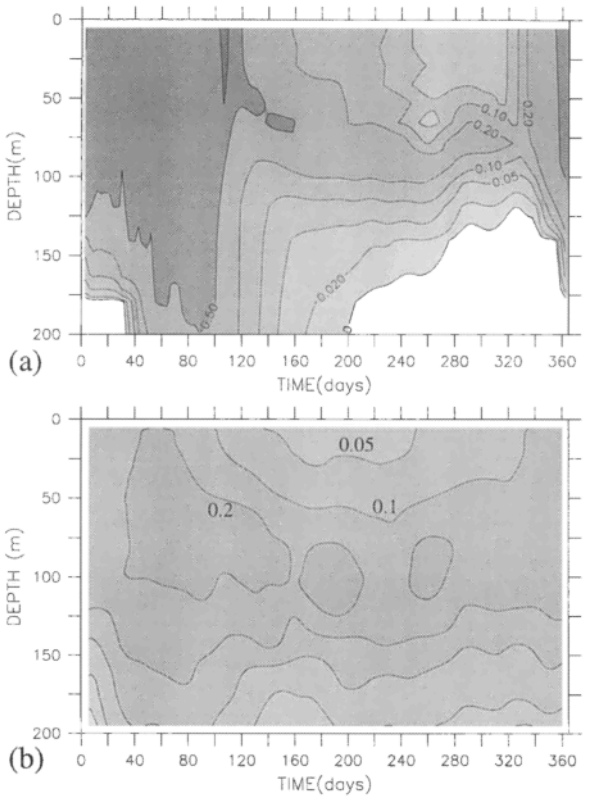

Figure 9. (a) Simulated and (b) observed annual cycle of chlorophyll at BATS (obtained via `http //www.bbsr.edu`). Observations are averaged over the years 1989 to 1996. Units are mg Chl m^{-3}. Isolines are drawn at 0.01, 0.1, 0.2, 0.5, 1.0, 2.0, and 5 0

mesoscale variability [*Oschlies and Garçon*, 1998]. This hints at deficiencies in the ecosystem model.

Sustaining primary production rates of 0.4 g C m^{-2} d^{-1} in the absence of measurable quantities of nitrate has repeatedly been reported to be problematic for simple pelagic ecosystem models [e.g., FAS93; *Doney et al*, 1996]. Models that emphasize the role of ammonium for regenerated production seem to be able to better simulate the summer mixed layer situation at BATS [e g , *Hurtt and Armstrong*, 1996]. Another possibly important mechanism so far neglected in the model is nitrogen fixation, that has for some time been discussed to be important to sustain the observed primary production in the Sargasso Sea in the absence of nitrate in summer [e.g., *Michaels et al.*, 1996; *Bissett et al.*, 1999].

With respect to the earlier model study presented by SAR93 and FAS93, the now available improved physical environment makes the model-data comparison a more stringent test for the ecosystem component. Winter nitrate concentrations are considerably lower and more realistic in the present model (1.4 mmol m^{-3} compared to >3.5 mmol NO_3 m^{-3} in FAS93). This also holds for maximum chlorophyll concentrations (1 2 mg m^{-3} versus 5.5 mg m^{-3}). These changes are consistent with an improvement in the physical environment. SAR93 attributed the elevated nitrate levels to an overly large contribution from the horizontal transport terms caused by unrealistically large upwelling of nutrient-rich water off the U.S. coast. This numerical artifact [*Veronis*, 1975] can be expected to be reduced on finer grids. As shown in Table 2, the annual nitrate input by horizontal advection in our model is on average 3 times smaller than the supply via vertical mixing, whereas horizontal advection dominated nitrate supply in FAS93's analysis. Despite this difference, and despite our model's capability to resolve mesoscale variability, nitrate input takes place mainly during winter in both models (for our model >90% from January until March), and the total amount of the annual supply is very similar in the two models (0.57 mol m^{-2} yr^{-1} reported by FAS93, 0.64 mol m^{-2} yr^{-1} in the present model). These values agree well with observational estimates of the annual new production [e.g., *Jenkins*, 1988]. However, the large contribution due to convective mixing in winter is in contrast to recent compilations of *McGillicuddy et al.* [1998] and *Siegel et al.* [1999], who suggest that eddy-induced nitrate fluxes are the dominant term in the annual mean. To clarify this issue, a more detailed analysis of mesoscale transport processes in the present high-resolution model is under way.

4.2. North Atlantic Bloom Experiment, 47°N Site

The North Atlantic Bloom Experiment (NABE) was a pilot process study of JGOFS. One of its central locations was the 47°N, 20°W site, chosen because of the historical background provided by a number of previous oceanographic [*Kupferman et al.*, 1986; *Mittelstaedt*, 1987] and biological [*Lochte and Pfannkuche*, 1987] investigations and because of the expected regular occurrence of a spring bloom. Model results at this site are compared with observations taken mainly during NABE in 1989. At present, we cannot rule out that 1989 was in any respect an "atypical" year which would make a comparison with a climatologically forced model problematic at least. However, model experiments with realistic daily forcing over the period 1989–1993, which will be presented elsewhere, suggest that 1989 indeed represents a "typical" year.

Main integral results of the coupled model at this site are given in Table 2 and Figure 4. Annual primary production (1.36 mol N m^{-2}) is slightly higher than at BATS, whereas nitrate supply and PON export both are lower at the NABE 47°N site. The latter difference is partly an artifact of the chosen level of 126 m across which the nitrogen fluxes are computed. At 47°N the euphotic zone in general is shallower than at BATS, so that a larger portion of recycling takes place already

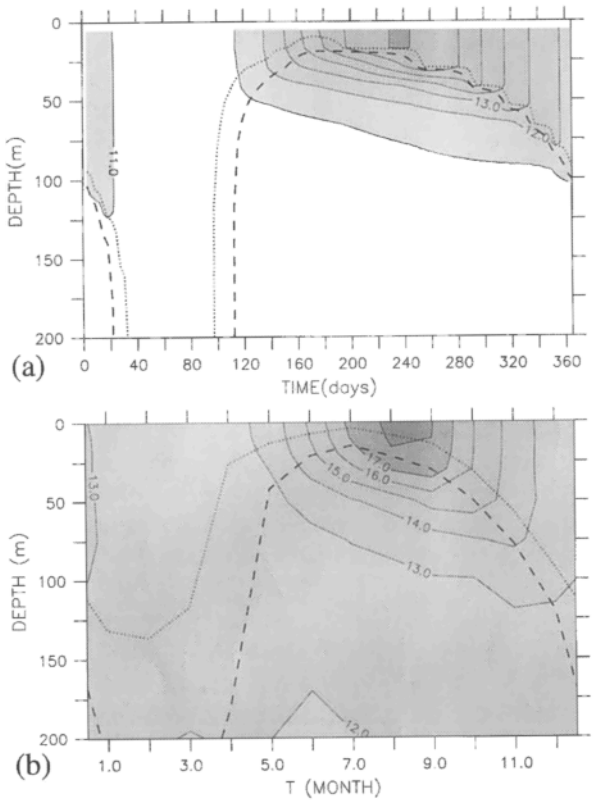

Figure 10. Annual cycle of temperature in the upper 200 m at the NABE 47°N site. (a) As simulated by the model; (b) as deduced from the *Levitus and Boyer* [1994] monthly climatolgy. Contour interval is 1°C, and the dotted and dashed lines indicate the depth where temperature deviates by 0.1°C and 0.5°C from the surface temperature.

above 126 m. Also in contrast to BATS is that PON export in the model occurs almost exclusively via the actively sinking detritus compartment. Even more pronounced than at BATS is the role of zooplankton grazing as the dominant phytoplankton loss term.

4.2.1. Seasonal cycle of the mixed layer. Figure 10 shows the simulated annual cycle of upper ocean temperature and the MLD at the 47°N site. Compared with the *Levitus and Boyer* [1994] climatology, simulated temperatures are too low by about 1.5°C during all seasons. In fact, the model underestimates surface temperatures over large parts of the eastern subpolar North Atlantic. This is related to the simulated path of the North Atlantic Current (NAC) that does not penetrate far enough eastward [e.g., *Oschlies and Willebrand*, 1996]. Because of the closed northern boundary, Denmark Strait overflow water that flows south at depth has to be compensated at the surface by a northward flow to the west of Iceland. Instead of leaving the model domain mostly to the east of Iceland, the relatively warm surface waters transported by the NAC flow northward mainly to the west of the Mid-Atlantic Ridge. As a consequence, the NAC's heat transport into the eastern subpolar North Atlantic is underestimated This is only partly compensated by a slight increase in surface heat fluxes in response to the too low SSTs (OG99, their Figure 7).

Since the ecosystem equations include only a weak dependence of the growth rate on temperature (OG99), a temperature offset is not critical to our results as long as it does not affect stratification and hence turbulent vertical mixing. The simulated seasonal cycle of the mixed layer extends down to about 700 m (both MLD criteria), whereas not more than 130 m (ΔT = 0 1°C) and 300 m (ΔT = 0.5°C) are reached in the *Levitus and Boyer* [1994] data (Figure 10). Using the *Robinson et al.* [1979] atlas, *Garside and Garside* [1993] deduce a MLD of 500 m at the NABE 47°N site. It is stressed again that estimates of the winter MLD from climatologies and climatologically forced models are not strictly comparable because of the smoothing of extreme events in climatological averages, for example, due to interannual variability in the time of deepest mixing. It is thus presently not clear to what extent the apparent overestimation of winter MLDs can be explained by the model's NAC transporting too little heat (and hence buoyancy) into the eastern subpolar North Atlantic or whether it is due to a smoothing effect in climatological data sets

Important for the correct simulation of ecosystem dynamics is that in response to surface warming in spring, both model and data show a deep ($\geq$300 m) winter mixed layer being capped by a shallow ($\leq$40 m) surface layer, thereby setting the physical environment for a spring bloom [*Sverdrup*, 1953]. In the model this rapid shallowing occurs around day 95. Observations during NABE in 1989 began at day 115 just before the start of a bloom around day 120 [*Marra and Ho*, 1993]. Numerical experiments with realistic synoptic forcing reveal that the beginning of the North Atlantic spring bloom can vary in time by several weeks depending on the atmospheric heat and momentum fluxes. The onset of the simulated spring bloom peaks agrees well with observations when daily forcing from the European Centre for Medium-Range Weather Forecasts (ECMWF) reanalysis for the year 1989 is used. The obvious time lag between the bloom in the present climatologically forced version of the model and the observations taken mainly in the spring of 1989 may therefore be attributed to the climatological atmospheric forcing used.

4.2.2. Prebloom phase. As can be deduced from Table 2, nitrate supply to the upper 126 m occurs mainly through vertical mixing. The annual cycle of the individual pathways of nitrate to the euphotic zone (Figure 11) shows that this takes place almost exclusively during early winter when the mixed layer is still deepening. With nitrate concentrations generally increasing with depth, it is evident that any overestimation of the winter MLD will result in overestimated surface nitrate

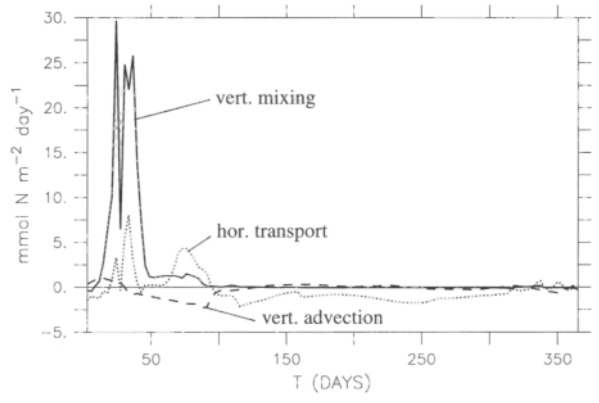

Figure 11. Annual cycle of nitrate input into the upper 126 m at the NABE 47°N site for turbulent vertical diffusion, and horizontal and vertical advection, respectively.

concentrations before the onset of the spring bloom. The nitrate field used to initialize the model [*Conkright et al*, 1994] yields 9.4 mmol m^{-3} when averaged (i.e., mixed) over the top 350 m, and 13.3 mmol m^{-3} when averaged over the upper 700 m. The latter value is reproduced almost identically in the winter of the third coupled year (Figure 12a). Unfortunately, there are no winter measurements of nitrate at the NABE 47°N site available. *Honjo et al.* [1989] report surface values of 9 4–9.8 mmol NO_3 m^{-3} measured on April 3, 1989, about 100 km farther to the north. As discussed by *Gardner et al.* [1993], this (together with simultaneous observations of particulate matter concentrations) indicates that significant primary production must have occurred before April 25 when the main observational phase of NABE began and when surface nitrate levels were already below 6 mmol NO_3 m^{-3} [*Marra and Ho*, 1993]. Only *Glover and Brewer* [1988] and *Garside and Garside* [1993] estimated winter nitrate concentrations larger than 10 mmol m^{-3} using a vertical extrapolation method. Koeve (Wintertime nutrients in the North Atlantic, I, New approaches and implications for estimates of seasonal new production, submitted to *Mar. Chem.*, 1999) gives a detailed discussion of different methods used to estimate prebloom nitrate concentrations at the NABE 47°N site. He concludes that for 1988–1992 winter values were not higher than 8 mmol NO_3 m^{-3} with an uncertainty of 15%. Obviously, simulated prebloom nitrate concentrations that exceed 13 mmol m^{-3} are too high. This is mainly a result of the overestimated winter mixed layer depth, although the relatively high vertically averaged concentrations obtained from the *Conkright et al.* [1994] data cited above also point to some uncertaintes in the initialization of nitrate in the model.

Phytoplankton growth rates are displayed in Figure 13a In winter, growth is limited by light, and when averaged over the deep winter mixed layer, it is not sufficient to balance the ecosystem model's constant phytoplankton mortality of 0.03 d^{-1} (Figure 13b). Consequently, standing stocks of phytoplankton, as well as of zooplankton and detritus, decrease during winter to reach minimum values at the end of March (day 85, Figure 14a). The corresponding primary production is as low as 0.6 mmol N m^{-2} d^{-1} (Figure 14b). Lowest prebloom primary production values observed during NABE were about 6 mmol N m^{-2} d^{-1} [*Lochte et*

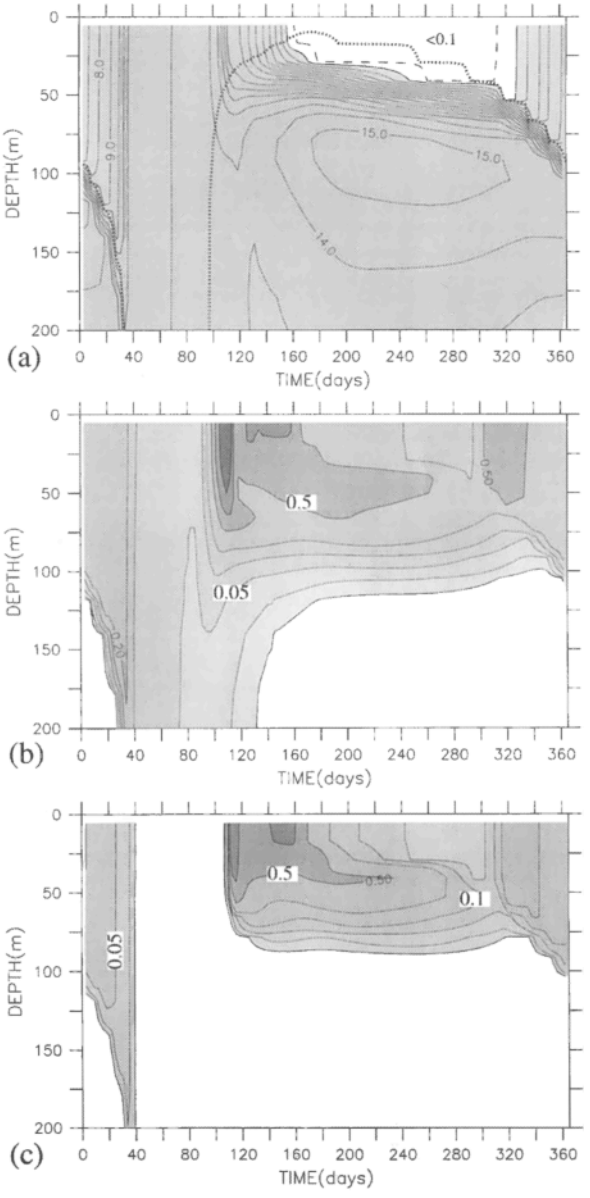

Figure 12. Simulated annual cycle of (a) nitrate, (b) chlorophyll, and (c) zooplankton in the upper 200 m at the NABE 47°N site (47°N, 20°W). The contour interval is 1.0 mmol m^{-3} in Figure 12a. Isolines in Figures 12b and 12c are drawn at 0.01, 0.02, 0.05, 0.1, 0 2, 0 5, 1 0, 2.0, and 5 0, with units mg Chl m^{-3} in Figure 12b, and mmol N m^{-3} in Figure 12c

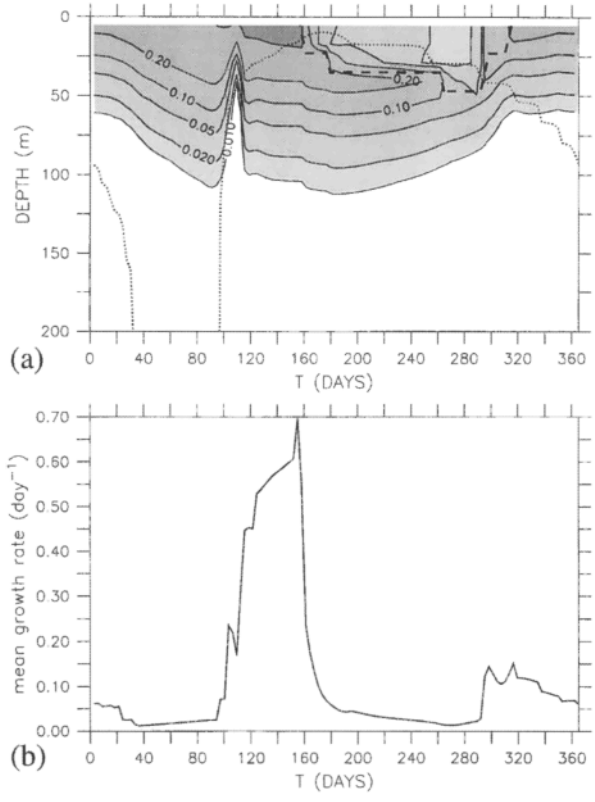

Figure 13. (a) Simulated phytoplankton growth rate at the NABE 47°N site (47°N, 20°W). Isolines at 0 01, 0.02, 0.05, 0.1, 0.2, and 0.5 day^{-1}. Regions above the heavy dashed line denote nutrient-limited growth, and elsewhere growth is light-limited. The dotted line refers to the bottom of the mixed layer defined by a $\Delta T = 0.1°C$ criterion. (b) Simulated phytoplankton growth averaged over the surface mixed layer indicated in Figure 13a.

al, 1993], taken only at the end of April. Presently, there are no earlier winter data available.

4.2.3. Spring bloom phase. The simulated spring bloom at the NABE 47°N site begins around day 95, initiated by the rapid shallowing of the surface mixed layer that results in a sharp increase in mixed-layer averaged growth rates to values larger than 0.5 d^{-1} (Figure 13). Primary production increases simultaneously with phytoplankton biomass to reach maximum values of 24 mmol N m^{-2} d^{-1} and 145 mmol N m^{-2}, respectively, around day 110 (Figure 14). This evolution agrees well with ^{14}C measurements taken during NABE: *Lochte et al.* [1993] report maximum primary production rates of 14-24 mmol N m^{-2} d^{-1} about 15 days after the onset of the bloom and maximum phytoplankton stocks of 90-110 mmol N m^{-2}. A closer analysis of the observations taken during the 1989 NABE study suggests that there was a sequence of two blooms, though spatial variability might have contributed to this signal [*Fasham and Evans*, 1995]

At the end of the initial spring bloom, nitrate concentrations are well above the half-saturation constant for phytoplankton growth, both in the model as well as in the observations [e.g., *Sieracki et al.*, 1993]. During this period the model ecosystem is thus insensitive to the possible overestimation of prebloom nitrate concentrations discussed above. However, this also means that maximum phytoplankton biomass must be controlled by another limiting nutrient (e.g., silicate), by grazing, aggregation, or mortality. Phytoplankton species counts show that the initial phase of the bloom is dominated by diatoms [*Lochte et al.*, 1993] what is consistent with the observed decline of silicate concentrations

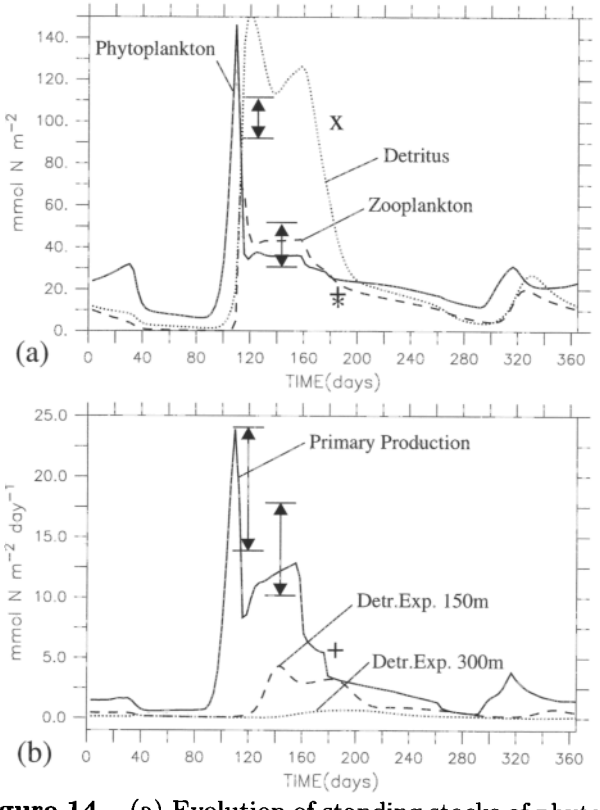

Figure 14. (a) Evolution of standing stocks of phytoplankton and zooplankton and of detritus at the NABE 47°N site, integrated over the top 100 m. Vertical bar refers to the phytoplankton chlorophyll measurements reported by *Lochte et al.* [1993] for the upper 80 m Symbols at day 185 represent 0-100 m standing stock integrals of *Weeks et al.* [1993], where the plus is phytoplankton, the asterisk is is zooplankton, and the cross is PON other than phytoplankton or zooplankton (i e, detrital material). (b) Annual cycle of primary production (integrated over the upper 300 m) and PON export out of the upper 150 and 300 m, respectively. Vertical bars refer to the primary production measurements described by *Lochte et al.* [1993] for different phases of the 1989 spring bloom. The cross denotes the primary production reported by *Weeks et al.* [1993]. Measurements were converted from carbon to nitrogen by a standard Redfield ratio of 6 625

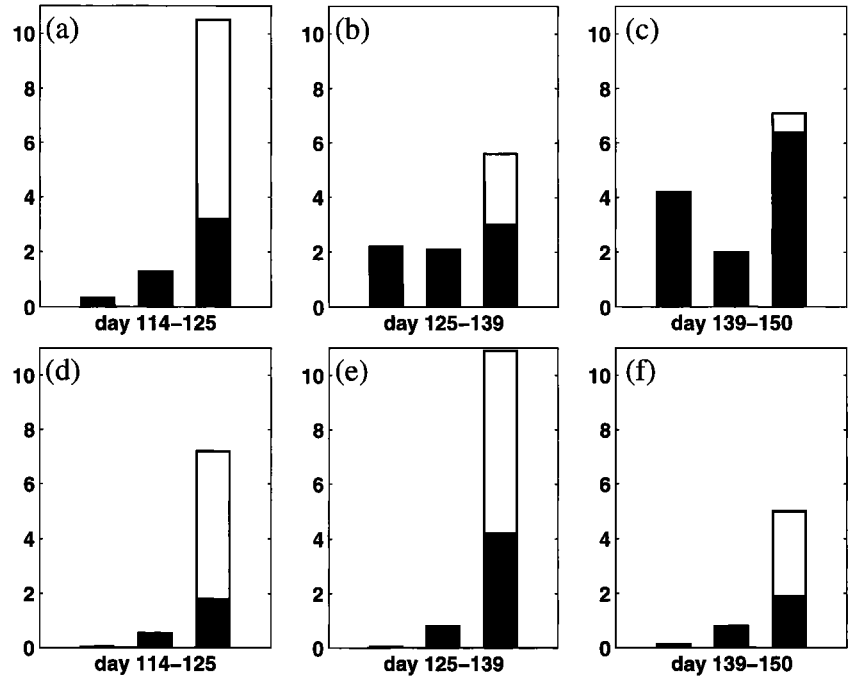

Figure 15. Particulate nitrogen export (a-c) at 150 m and (d-f) at 300 m at the NABE 47°N site. The first column represents model results, the second denotes trap measurements reported by *Martin et al.* [1993], and the third one shows both the high and low flux estimates from the ^{234}Th scavenging model of *Buesseler et al.* [1992].

[*Sieracki et al.*, 1993]. In the present model, which has only nitrate as potentially limiting nutrient, aggregation is not explicitly accounted for and phytoplankton mortality is held constantly at 0.03 day^{-1}, that is, more than an order of magnitude less than the maximum growth rates depicted in Figure 13. Consequently, only grazing by zooplankton is left to balance phytoplankton growth in spring. Initial test experiments (reported by OG99) had indeed revealed a marked sensitivity of spring-bloom phytoplankton concentrations to the maximum grazing parameter. As shown in Figure 14a, zooplankton biomass peaks about 5 days after phytoplankton, indicating a quick response to changes in food availability. To the extent that the initial bloom consists of diatoms, one would expect that mesozooplankter would be the dominant grazers. A quick response of mesozooplankton is, however, not confirmed by observations taken during NABE [*Dam et al.*, 1993]. Between days 120 and 160 the model shows a second increase in primary production which may be viewed as a second bloom, or as *Lochte et al.* [1993] put it, another phase of the spring bloom. During this phase, flagellates dominated and grazing occured mainly via microzooplankton [*Verity et al.*, 1993]. Consistent with the observations [e.g., *Lochte et al.*, 1993], the model simulates relatively constant standing stocks of phytoplankton.

Particle export at the 47°N site was estimated via shallow sediment traps [*Martin et al.*, 1993] and via a non-steady state ^{234}Th scavenging model [*Buesseler et al.*, 1992]. While the latter method produced significantly higher fluxes, the difference between the two estimates has not been fully resolved [*Martin et al.*, 1993; *Buesseler et al.*, 1992]. As shown in Figure 15, export rates simulated by our model agree rather well with the observations at 150 m, but are consistently lower than either observational estimate at 300 m. This indicates a too shallow remineralization which may be caused by a too slow settling velocity (5 m d^{-1}) or too high rates of detritus remineralization.

4.2.4. Postbloom phase. *Garside and Garside* [1993] report that surface nitrate was just above detection limit (0.1 mmol m^{-3}) at the end of May (day 151), after having declined from about 2 mmol m^{-3} during the previous 2 weeks. In the model, surface nitrate becomes depleted (<0.1 mmol m^{-3}) after day 156 (Figure 12a). This is associated with a rapid decline of growth rates within the surface mixed layer (Figure 13b). Growth rates are still relatively high in the nitracline (Figure 13a), giving rise to the development of a subsurface maximum of phytoplankton biomass and hence chlorophyll (Figure 12b). Depth (30-60 m) and intensity (0.7-0.9 mg Chl m^{-3}) of the subsurface maximum agree roughly with observations of *Joint et al.* [1993], taken

around day 185 (1.0-1.5 mg Chl m^{-3} at 30–40 m). Note that the deep chlorophyll maximum in the real ocean is a combined effect of enhanced new production at the nitracline [*Eppley and Koeve*, 1990; *Koeve et al.*, 1993] and an adaptation to low light levels [*Cullen*, 1982]. The latter effect is not accounted for in the model.

Simulated postbloom zooplankton standing stocks are similar to those of phytoplankton. This is consistent with the findings of *Weeks et al.* [1993]. Our simulation also agrees with their observations (indicated as crosses in Figure 14a) that detrital material makes up for more than two thirds of total POC in the upper 100 m. Primary production declines steadily from 12.5 mmol N m^{-2} d^{-1} at day 156 to less than 1 mmol N m^{-2} d^{-1} around day 290 (Figure 14b). This seems to be consistent with the measurements of *Weeks et al.* [1993] and *Veldhuis et al.* [1993] who report values between 290 and 430 mg C m^{-2} d^{-1} (3.6 to 5.4 mmol N m^{-2} d^{-1}) after day 180.

In the model there is a secondary maximum both in standing stocks as well as in primary production (Figure 14) in autumn. The deepening of the mixed layer entrains nitrate (Figures 10 and 12a) and leads to an increase of phytoplankton growth rates (Figure 13). This renewed nitrate supply does not show up in Figure 11 because all the turbulent transport takes place above the 126 m level. A small bloom develops and is followed by an increase of zooplankton concentrations (Figure 14a). Mixed layer averaged growth rates stay above 0.05 day^{-1} until the end of the year, before mixing becomes too deep to allow for phytoplankton growth to exceed mortality. Observations during NABE did not cover this season, but monthly mean CZCS data [*Esaias et al.*, 1986] also indicate the occurrence of an autumn bloom at the NABE 47° site.

4.2.5. Summary: NABE 47°N. There is generally good agreement between simulated and observed phytoplankton stocks and rates of primary production at the NABE 47°N site. Obviously, the model is able to switch from the biomass-accumulating first phase of the bloom to a phase with rather constant POC stocks. Without aggregation being included in the model, the transition is triggered through the development of a large zooplankton peak. While there are no microzooplankton observations available during the initial phase of the bloom, there is no evidence for a mesozooplankton peak in the observations [*Dam et al.*, 1993] that could have efficiently reduced the large diatom stock. Instead, the switch describing the rapid disappearance of (particularly) diatoms which are subsequently replaced by small phytoflagellates and cyanobacteria is associated with higher settling fluxes found in shallow particle traps [*Buesseler et al.*, 1992]. It is well established that a fraction of the diatom phytoplankton bloom is exported rapidly to great depth [*Billet et al.*, 1983; *Pfannkuche*, 1993; *Honjo and Manganini*, 1993] and it has been suggested that aggregation of phytoplankton is an important source of fast sinking particles [*Alldredge and Gotschalk*, 1989; *Lampitt et al.*, 1993]. We cannot expect that a model with constant (5 m d^{-1}) sinking velocity can adequately reproduce such export pulses to the deep ocean. Nevertheless, even the present configuration can give a quite realistic description of upper ocean (~0–150 m) nitrogen cycling at the NABE 47°N site, to the extent that we have to allow for a probably unrealistically high zooplankton grazing (Figure 4).

4.3. EUMELI Oligotrophic Site

Between July 1989 and December 1992, five cruises were carried out within the French Eutrophic, Mesotrophic, Oligotrophic (EUMELI) program at about 20°N in the eastern subtropical Atlantic. Of most interest to the present study is the oligotrophic site near 21°N, 31°W because it is nearest to the interior of the subtropical gyre where our model simulates primary production rates much smaller than deduced from the CZCS data (section 3.2 and Figure 3). The site is situated to the north of the North Equatorial Current (NEC) in the rather quiet southeastern periphery of the subtropical gyre, though some mesoscale variability associated with the NEC meandering can be expected [*Dadou et al.*, 1996].

As Table 2 reveals, simulated annual primary production at this site is less than 0.05 mol N m^{-2} (4 g C m^{-2}) which is more than an order of magnitude smaller than the satellite-derived estimates of Figure 3 would suggest. Note the relatively large contribution of horizontally advected phytoplankton and zooplankton to the total nitrogen input into the upper 126 m at the EUMELI site (5 times the input of nitrate!). Figure 4 further shows that zooplankton is relatively unimportant in the flow of nitrogen through the simulated ecosystem. In contrast to the model behavior at both the BATS and NABE 47°N sites, at EUMELI phytoplankton loss almost exclusively takes the direct route ("mortality") to detritus.

4.3.1. Physical properties. An overview of the hydrographic environment of the EUMELI stations is given by *Morel* [1999]. At the oligotrophic site, winter temperatures are generally above 22°C, and mixing does not penetrate deeper than about 120 m. This is well reproduced by the model, as are summer MLDs of about 50 m with maximum temperatures of about 26°C (Figure 16). Simulated temperatures are in general slightly higher (by about 0.5°C) than the *Levitus and Boyer* [1994] data shown in Figure 16b.

4.3.2. Biogeochemical and biological structures. The observations show no measurable levels of nitrate in the upper 90 m during all seasons. This is well reproduced by the model (Figure 17a) as well as the

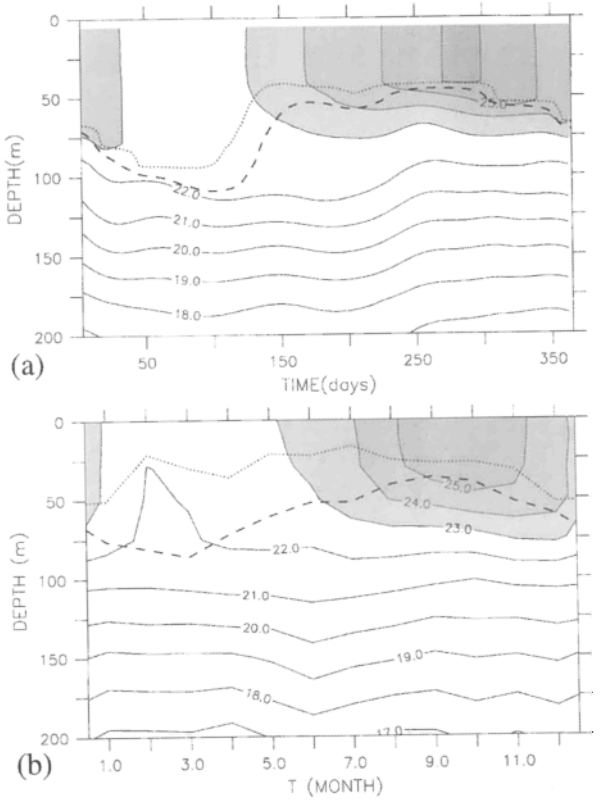

Figure 16. Annual cycle of temperature in the upper 200 m at 20°N, 30°W. (a) As simulated by the model; (b) as deduced from the *Levitus and Boyer* [1994] monthly climatolgy. Contour interval is 1°C, and the dotted and dashed lines indicate the depth where temperature deviates by 0.1°C and 0.5°C from the surface temperature.

fact that this nitrate-depleted layer is generally deeper than the surface mixed layer. Even winter mixing does not penetrate the nitracline, explaining the absence of a spring bloom and a pronounced seasonal cycle. Only at about day 40 there is a deepening of the mixed layer that just touches the 0.1 mmol NO_3 m^{-3} surface. The associated short increase of growth rates to values above 0.05 day^{-1} (Figure 18) does, however, not lead to a noticeable increase of phytoplankton biomass. Simulated standing stocks, displayed in Figure 19, show a larger increase in phytoplankton between days 80 and 120 and also around day 240. During these events, biomass approximately doubles over 30 days. If produced locally, this would require phytoplankton growth rates larger than 0.05 day^{-1} (taking into account the constant mortality of 0.03 day^{-1}). The fact that model-generated growth rates are consistently lower at the EUMELI oligotrophic site (Figure 18) immediately points to horizontal advection as the only remaining source of plankton (see Table 2 and Figure 4).

A closer inspection of the model results reveals meanders of the NEC passing by the site during these times. Figure 20 shows the surface chlorophyll field and current velocities (at $z = 100$ m to avoid contamination by the ageostrophic Ekman flow) at day 105, when a current band of the southwestward flowing NEC has formed a large cyclonic meander with elevated surface chlorophyll concentrations just to the northwest of the EUMELI oligotrophic site. A meridional section along 30°W shows the doming of NO_3 isolines as well as of the base of the mixed layer in regions of cyclonic flow

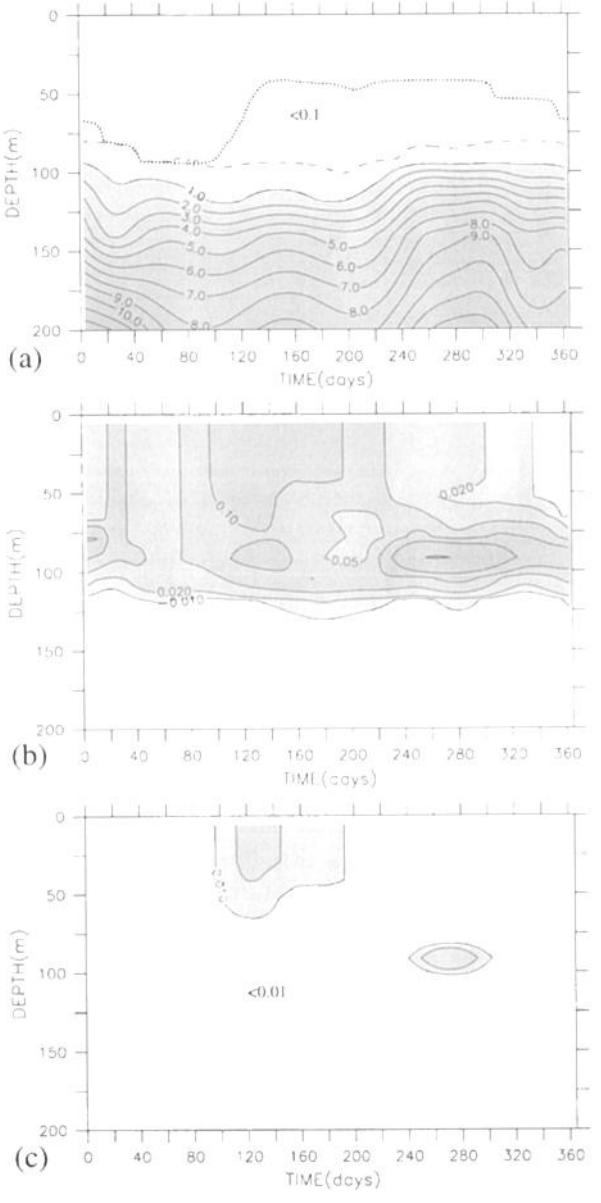

Figure 17. Simulated annual cycle of (a) nitrate (in mmol m^{-3}), (b) chlorophyll (in mg Chl m^{-3}, using a constant ratio of 1.59 mg Chl (mmol N)$^{-1}$), and (c) zooplankton (in mmol N m^{-3}) in the upper 200 m near the EUMELI oligotrophic site at 20°N, 30°W. Isolines in Figures 17b and 17c are at the 0.01, 0.02, 0.05, 0.1, and 0.2 levels.

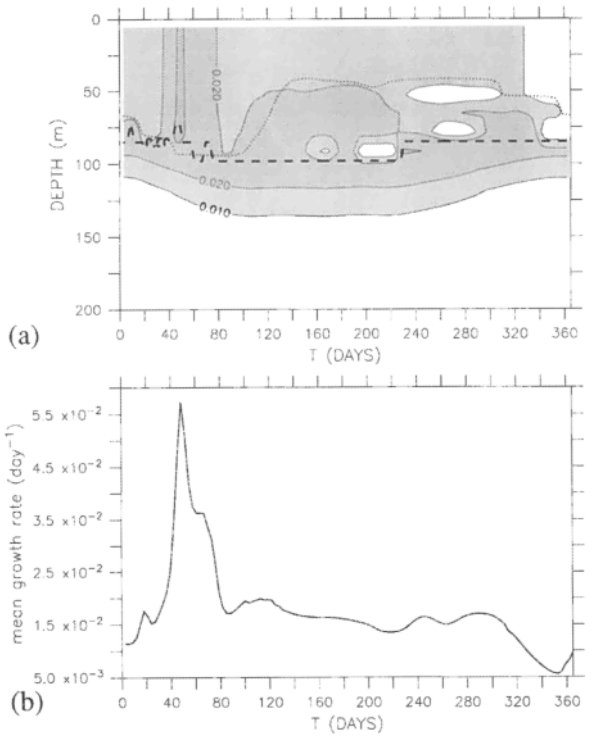

Figure 18. Simulated phytoplankton growth rate near the EUMELI oligotrophic site at 20°N, 30°W. Isolines at 0.01, 0.02, and 0.05 day^{-1}. Regions above the heavy dashed line denote nutrient-limited growth, and elsewhere growth is light-limited.

at 18°–19°N, near 21°N, and also at 24°N. Note that the general north-south gradient in the nitrate field below the mixed layer, associated with the Cape Verde Frontal Zone [*Zenk et al.*, 1991], leads to different responses of the ecosystem model in the respective cyclonic features.

All EUMELI cruises found a deep chlorophyll maximum (DCM) at the nitracline at or slightly below 100 m [*Morel*, 1999]. The depth of the DCM is accurately represented by the model (Figure 17b). Observed DCM concentrations range from 0.25 to 0.45 mg Chl m^{-3}. Using the standard conversion factor of 1.59 mg Chl per mol nitrogen, simulated values are in general too small by a factor 2 or more (Figure 17b). The model reaches chlorophyll concentrations larger than 0.2 mg Chl m^{-3} (in the maximum even exceeding 0.5 mg Chl m^{-3}) only between days 240 and 320.

A similar picture holds for the vertically integrated biomass. Simulated phytoplankton biomass does not exceed 9 mmol N m^{-2}. The integrated chlorophyll value given by *Morel* [1999] (23.6 mg Chl m^{-2}, or, using the standard conversion, 14.8 mmol N m^{-2}) indicate an underestimation by the model by a factor of about 2. *Morel* [1999] reports two estimates of vertically (0–200 m) integrated mesozooplankton biomass at the EUMELI oligotrophic site. 205 and 370 mg C m^{-2}. These are included in Figure 19. Maximum zooplankton biomass in the model reaches 125 mg C m^{-2} (using C N= 6.625 to convert nitrogen to carbon). However, a direct comparison of mesozooplankton measurements with the single zooplankton compartment of the model is problematic, particularly in oligotrophic regions where small size classes tend to dominate the food web.

While simulated phytoplankton agrees with the observations within a factor of about 2, considerably larger discrepancies are found for primary production rates Simulated daily production is always less than 0 25 mmol N m^{-2} (20 mg C m^{-2}) (Figure 19b) which is an order of magnitude less than has been measured in situ [*Morel*, 1999]. Figure 19b further reveals that a rather large portion (on average 70%) of the pri-

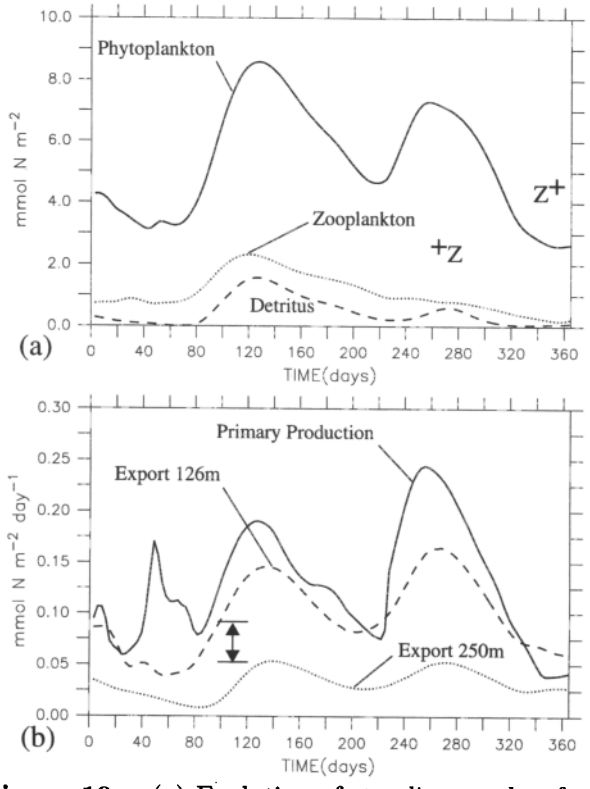

Figure 19. (a) Evolution of standing stocks of phytoplankton and zooplankton and of detritus close to the EUMELI oligotrophic site, integrated over the top 100 m. Crosses refer to mesozooplankton meassurements reported by *Morel* [1999]. When the chlorophyll data of *Morel* [1999] are converted to nitrogen using 1.59 mg Chl (mmol N)$^{-1}$, these correspond to values between 13.4 and 15.7 mmol N m^{-2}. (b) Annual cycle of primary production (integrated over the upper 300 m) and PON export out of the upper 150 and 250 m, respectively. The vertical bar refers to measurements of POC export in sediment traps at 250 m (N. Leblond, personal communication, 1999; H. Etcheber, personal communication, 1999) converted to PON flux by a standard ratio of 6 625

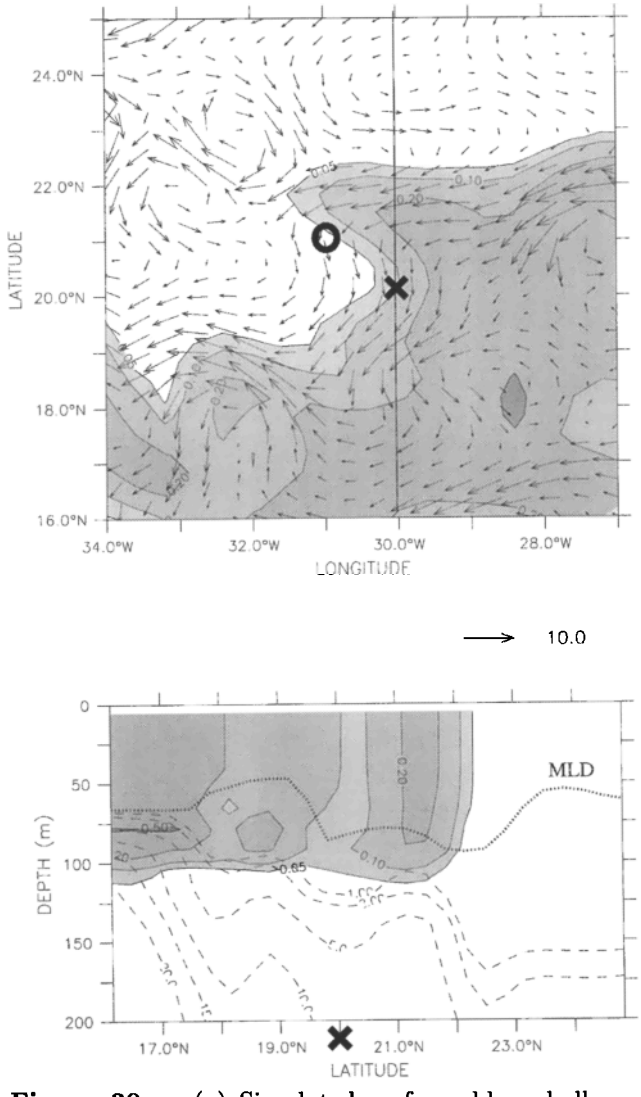

Figure 20. (a) Simulated surface chlorophyll near the EUMELI oligotrophic site. Isolines are at 0.05, 0.1, 0 2, and 0.5 mg Chl m^{-3}. Current vectors represent the horizontal velocity at a depth of 100 m. A velocity of 10 cm s^{-1} is indicated by the arrow below. The circle indicates the site of the traps during the EUMELI program, and the cross denotes the grid point at which the model results were stored. (Since grid points along 30°W have for a long time routinely been used for model analysis, we desisted from setting up another analysis grid point closer to the actual EUMELI oligotrophic site) (b) Vertical section along 30°W (indicated in Figure 20a) of chlorophyll, mixed layer depth (MLD), and nitrate (dashed lines).

mary production is exported as detritus across the 126 m depth level which we have chosen as proxy for the depth of the euphotic zone. An f ratio of 0.7 is much larger than the observational estimates of 0.1–0 18 reported by *Morel* [1999]. Only few data of shallow POM export are available: data from a sediment trap at 250 m [*N. Leblond*, personal communication, 1999, *H Etcheber*, personal communication, 1999] are included in Figure 19b. The order-of-magnitude agreement with these data suggests that the model simulates shallow particle export much better than primary production.

4.3.3. Summary: EUMELI. Agreement between simulated and observed stocks of nitrate and chlorophyll is relatively good, with some tendency of the model to underestimate plankton biomass by about a factor of 2. At the same time, the simulated primary production is too low by an order of magnitude Simulated particle export, on the other hand, is not inconsistent with the few data available from shallow traps. Together with the unrealistically high f ratio of about 0.7 in the model, this indicates that the simulated recycling of nutrients in the euphotic zone is too inefficient under oligotrophic conditions. In the same direction points the extremely small role of zooplankton in the simulated food web (Figure 4). Almost all phytoplankton loss goes directly to detritus, of which about half sinks out of the euphotic zone and hence is not available for recycling.

5. Discussion

The maps of surface chlorophyll and primary production, presented in section 3 of the paper, demonstrate that the main patterns and geographical distributions of biological provinces as defined by *Longhurst* [1995] are well reproduced by coupling a simple NPZD ecosystem model with a uniform set of biological parameters to a basin-scale eddy-permitting model. This is consistent with previous model studies [e.g., *Sarmiento et al*, 1993] and underlines the important role of the physical environment in controlling ecosystem dynamics in the ocean.

In order to reach a more quantitative assessment of the coupled model's performance, data from three JGOFS local study sites in different biogeochemical provinces have been used: BATS in the western part of the subtropical gyre, NABE 47°N in the North Atlantic drift region, and EUMELI in the trade wind domain This led to the identification of two principal model deficiencies. On the one hand, primary production was found to be much too low at EUMELI where phytoplankton stocks seem to agree within a factor of 2, but where simulated zooplankton was surprisingly inactive On the other hand, simulated phytoplankton and zooplankton biomass was too large during the spring bloom at the BATS and NABE 47° sites, where primary production rates were in good agreement with the data Moreover, the modeled spring bloom could be terminated only by an unrealistically rapid development of a large zooplankton stock. In the following, we will address the problems in oligotrophic and bloom situations separately

5.1. Oligotrophic Situation

When we set up the high (1/3°) resolution coupled ecosystem-circulation model, we did not anticipate that primary production in the subtropical gyre would remain relatively unchanged with respect to the results obtained by SAR93 using a much coarser (2°) model. Despite the more realistic simulation of mesoscale variability, which was shown to contribute more than one third of the nitrate supply in the subtropics and midlatitudes [*Oschlies and Garçon*, 1998], primary production still is smaller than CZCS-derived estimates by more than an order of magnitude in the subtropical gyre (Figure 3).

While satellite-derived estimates of primary production depend on model assumptions themselves, a comparison with in situ observations at the EUMELI oligotrophic site left little doubt on the seriousness of the model's failure. On the basis of a comparison with biomass standing stocks as well as primary and export production it was concluded that the simulated recycling of nutrients in the euphotic zone was too inefficient. This judgement is consistent with the results obtained at BATS. Here simulated primary production was also found to be systematically underestimated during the oligotrophic summer period.

To improve the model results in oligotrophic regions, a more efficient representation is needed of the recycling that takes place within the euphotic zone and that fuels regenerated production. While the present model configuration at EUMELI behaves almost like an NPD model (Figure 4), one could attempt to strengthen the role of zooplankton. This strategy, however, is opposed by the general model structure. The chosen formulation of the zooplankton grazing (equation (6)) in combination with a linear term for excretion (equation (2)) sets a lower limit for net zooplankton growth. For small zooplankton concentrations we can, to leading order, neglect the quadratic zooplankton loss term $\mu_Z Z^2$ in the zooplankton equation that describes grazing by higher trophic levels. This results in a critical phytoplankton concentration below which a zooplankton population can not be maintained without input via advection or diffusion:

$$P_{\mathrm{crit}} = \left(\frac{\gamma_2 g}{(\gamma_1 g - \gamma_2)\epsilon} \right)^{\frac{1}{2}} \qquad (7)$$

For the parameters used (Table 1) this threshold concentration of phytoplankton amounts to $P_{\mathrm{crit}} = 0.2$ mmol N m^{-3} (or 0.3 mg Chl m^{-3}). At lower concentrations, zooplankton loss terms dominate.

The existence of a threshold phytoplankton concentration necessary for net zooplankton growth is a result of combining a Holling-type III grazing function with a linear zooplankton loss term. The situation would not be much different for a Holling-typ II (e.g., SAR93, FAS93) or Ivlev grazing [e.g., *Doney et al.*, 1996] functions. The problem is instead tied to the existence of a linear zooplankton loss term (here called excretion) that is widely used in pelagic ecosystem models [*Evans and Garçon*, 1997]. More work (and possibly more zooplankton data than obtained within JGOFS) will be needed to refine the formulation of zooplankton in such models.

For the present, a more pragmatic approach of enhancing the regenerated production without introducing new model compartments (particularly important for computationally expensive 3-D models) may be the introduction of a direct fast recycling path from phytoplankton back to nitrate (which would then more appropriately be called "dissolved inorganic nitrogen" since it would include the ammonium pool). Work is under way to investigate whether this route can be appropriate for a basin-scale model.

5.2. Bloom Situation

Model deficiencies during the spring bloom were identified both at BATS and at the NABE 47°N site. At both sites, primary production was within observed ranges during the spring bloom, but phytoplankton and especially zooplankton biomass tended to be too high. This indicates an overestimation of grazing and an underestimation of other phytoplankton loss terms. At the NABE 47°N site where nitrate is not depleted until long after the initial bloom is over, the simulated bloom could only be terminated by grazing by a rapidly grown zooplankton stock for which there is no observational evidence.

Our suggestion for model improvement is to explicitly include aggregation. The subsequent export of phytoplankton could considerably improve the simulation of the spring bloom both at BATS and at the NABE 47°N. Since aggregation principally applies when phytoplankton concentrations are high, we would expect little effect of such an alteration of the ecosystem model in oligotrophic regimes. *Kriest and Evans* [1999] report promising results of including aggregation in zero-dimensional model simulations for various bloom scenarios. Presently, their aggregation routine is prepared for implementation into the basin-scale 3-D model.

6. Conclusions

As already stated by FAS93 (p. 403), one of the major problems in evaluating the results of coupled ecosystem-circulation models is "to distinguish between deficiencies caused by the physical model and those caused by the ecological model." Here the considerable improvement in the model physics with respect to earlier coupled ecosystem-circulation studies, a combined effect of increased resolution, improved formulations of surface heat fluxes and mixed layer physics, and more accurate advection numerics, allows for a more rigorous assessment of the ecosystem model component. We

find that the main aspects of the seasonal cycle of surface chlorophyll are well reproduced by the model, as are spatial patterns of increased primary production in mid and high latitudes and in coastal upwelling regions. That is, the main biological provinces as defined by *Longhurst* [1995] can be distinguished by the model with a uniform set of ecosystem parameters.

A more detailed and quantitative comparison is carried out in different biological provinces using JGOFS time series and process study data at BATS, and at the NABE 47°N and the EUMELI oligotrophic sites. Good quantitative agreement is reached for the primary production during the spring bloom at BATS and NABE 47°N, whereas the simulated biomass agrees best with the observations in the postbloom phase as well as at the EUMELI oligotrophic site. The main deficiencies of the model are a considerable underestimation of primary production in oligotrophic situations and an overestimation of plankton biomass during the bloom both at BATS and NABE 47°N. The latter model shortcoming is related to the unrealistic termination of the phytoplankton spring bloom by a rapidly growing zooplankton stock.

To significantly improve the model results in oligotrophic regions, it is suggested to introduce a more efficient recycling loop that enhances regenerated production. Possible solutions include the introduction of the ammonium and microbial loops. To what extent these loops have to be modeled explicitly and to what extent implicit parameterizations may suffice is presently not clear. Related to this issue is the interpretation of the modeled zooplankton pool. Clearly, more regenerated production is not what is needed to improve the model during eutrophic bloom situations. However, while increasing the importance of recycling in the euphotic zone will affect both bloom scenarios as well as oligotrophic conditions, the other proposed model improvement, accounting for aggregation effects, will be felt only at high phytoplankton concentrations typical for blooms. It is thus hoped that a careful balance of both suggested model improvements will allow a more realistic simulation for different biological provinces simultaneously. One technically simple realisation might be to change the phytoplankton loss term to detritus from a linear function of phytoplankton concentration to a quadratic one. This would result in increasingly high loss of phytoplankton at high concentrations (i.e., bloom situations) and increasingly less loss at low concentrations (i.e., oligotrophic situations). Work is under way to investigate such an alternative model description. The results presented here and the model deficiencies detected leave us optimistic to further improve simple ecosystem models with unique parameter sets for entire ocean basins.

Acknowledgments.
We thank Rick Slater, David Antoine, and Mike Behrenfeld who generously made the gridded CZCS and primary production data available to us. Discussions with Iris Kriest and Markus Schartau and helpful comments of two anonymous reviewers helped to clarify the manuscript. A.O. and W.K. were supported by German JGOFS, and V.G. obtained support from the French JGOFS Modelling Project.

References

Alldredge, A. L., and C. C. Gotschalk, Direct observation of the mass flocculation of diatom blooms: Characteristics, settling velocities and formation of diatom aggregates, *Deep Sea Res., 36*, 159–171, 1989.

Altabet, M. A., Particulate new nitrogen fluxes in the Sargasso Sea, *J. Geophys. Res., 94*, 12,771–12,779, 1989.

Antoine, D., J.-M. André, and A. Morel, Oceanic primary production, 2, Estimation at global scale from satellite (coastal zone color scanner) chlorophyll, *Global Biogeochem. Cycles, 10*, 57–69, 1996.

Aumont, O., J. C. Orr, P. Monfray, G. Madec, and E. Maier-Reimer, Nutrient trapping in the equatorial Pacific: The ocean circulation solution, *Global Biogeochem. Cycles, 13*, 351–369, 1999.

Behrenfeld, M. J., and P. G. Falkowski, Photosynthetic rates derived from satellite-based chlorophyll concentration, *Limnol. Oceanogr., 42*, 1–20, 1997.

Berger, W. H., Global maps of ocean productivity, in *Productivity of the Ocean: Present and Past*, edited by W. H. Berger, V. S. Smetaceck, and G. Wefer, pp. 429–455, John Wiley, New York, 1989.

Billet, D. S. M., R. S. Lampitt, A. L. Rice, and R. F. C. Mantoura, Seasonal sedimentation of phytoplankton to the deep sea benthos, *Nature, 302*, 520–522, 1983.

Bissett, W. P., J. J. Walsh, D. A. Dieterle, and K. L. Carder, Carbon cycling in the upper water of the Sargasso Sea, I, Numerical simulation of differential carbon and nitrogen fluxes, *Deep Sea Res., Part I, 46*, 205–269, 1999.

Blanke, B., and P. Delecluse, Variability of the tropical Atlantic Ocean simulated by a general circulation model with two different mixed-layer physics, *J. Phys. Oceanogr. 23*, 1363–1388, 1993.

Böning, C. W., F. O. Bryan, W. R. Holland, and R. Döscher, Deep-water formation and meridional overturning in a high-resolution model of the North Atlantic, *J. Phys. Oceanogr., 26*, 1142–1164, 1996.

Bryan, F. O., and W. R. Holland, A high resolution simulation of the wind- and thermohaline-driven circulation in the North Atlantic Ocean, in *Parameterization of Small-Scale Processes*, edited by P. Müller and D. Henderson, pp. 99–115, Hawaii Inst. of Geophys., Manoa, 1989.

Buesseler, K. O., M. P. Bacon, J. K. Cochran, and H. D. Livingston, Carbon and nitrogen export during the JGOFS North Atlantic Bloom Experiment estimated from ^{234}Th:^{238}U disequilibria, *Deep Sea Res., 39*, 1115–1137, 1992.

Carlson, C. A., H. W. Ducklow, and A. F. Michaels, Annual flux of dissolved organic carbon from the euphotic zone in the northwestern Sargasso Sea, *Nature, 371*, 405–408, 1994.

Conkright, M. E., S. Levitus, and T. P. Boyer, *World Ocean Atlas 1994*, vol. 1, *Nutrients*, Natl. Environ. Satell. Data and Inf. Serv., Natl. Oceanic and Atmos. Admin., Silver Spring, Md., 1994.

Cullen, J. J., The deep chlorophyll maximum: Comparing vertical profiles of Chlorophyll-a, *Can. J. Fish. Aquat. Sci., 39*, 791–803, 1982.

Dadou, I., V. Garçon, V. Andersen, G. R. Flierl, and C. S. Davis, Impact of the North Equatorial Current meander-

ing on a pelagic ecosystem: A modeling approach, *J. Mar. Res., 54*, 311–342, 1996.

Dam, H. G., C. A. Miller, and S. H. Jonasdottir, The trophic role of mesozooplankton at 47°N, 20°W during the North Atlantic Bloom Experiment, *Deep Sea Res., Part II, 40*, 197–212, 1993.

Doney, S. C., D. M. Glover, and R. G. Najjar, A new coupled, one-dimensional biological-physical model for the upper ocean: Application to the JGOFS Bermuda Atlantic Time series Study (BATS) site, *Deep Sea Res., Part II, 43*, 591–624, 1996.

Ducklow, H. W., and R. P. Harris, Introduction to the JGOFS North Atlantic Bloom Experiment, *Deep Sea Res., Part II, 40*, 1–8, 1993.

Eppley, R. W., and W. Koeve, Nitrate use by plankton in the eastern subtropical North Atlantic, March–April 1989, *Limnol. Oceanogr., 35*, 1781–1788, 1990.

Esaias, W., G. C. Feldman, C. R. McClain, and J. A. Elrod, Monthly satellite-derived phytoplankton pigment distribution for the North Atlantic Ocean Basin, *Eos Trans. AGU, 67*, 835–837, 1986.

Evans, G. T., and V. C. Garçon, One-dimensional models of water column biology, *JGOFS Report 23*, SCOR, JGOFS Bergen, Norway, 85 pp., 1997.

Evans, G. T., and J. S. Parslow, A model of annual plankton cycles, *Biol. Oceanogr., 3*, 328–347, 1985.

Fasham, M. J. R., Variations in the seasonal cycle of biological production in subarctic oceans: A model sensitivity analysis, *Deep Sea Res., Part I, 42*, 1111–1149, 1995.

Fasham, M. J. R., and G. T. Evans, The use of optimisation techniques to model marine ecosystem dynamics at the JGOFS station at 47N 20W, *Philos. Trans. R. Soc. London, Ser. B, 348*, 203–209, 1995.

Fasham, M. J. R., J. L. Sarmiento, R. D. Slater, H. W. Ducklow, and R. Williams, Ecosystem behavior at Bermuda Station "S" and Ocean Weather Station "India": A general circulation model and observational analysis, *Global Biogeochem. Cycles, 7*, 379–415, 1993.

Feldman, G. C., et al., Ocean color, availability of the global data set, *Eos Trans. AGU, 70*, 633–648, 1989.

Fitzwater, S. E., G. A. Knauer, and J. H. Martin, Metal contamination and its effect on primary production measurements, *Limnol. Oceanogr., 27*, 544-551, 1982.

Gardner, W. D., I. D. Walsh, and M. J. Richardson, Biophysical forcing of particle production and distribution during a spring bloom in the North Atlantic, *Deep Sea Res., Part II, 40*, 171–195, 1993.

Garside, C., and J. C. Garside, The "f-ratio" on 20°W during the North Atlantic Bloom Experiment, *Deep Sea Res., Part II, 42*, 75–90, 1993.

Gaspar, P., Y. Gregoris, and J.-M. Lefevre, A simple eddy kinetic energy model for simulations of the oceanic vertical mixing: Tests at station Papa and Long–Term Upper Ocean Study site, *J. Geophys. Res., 95*, 16,179–16,193, 1990.

Glover, D. M., and P. G. Brewer, Estimates of wintertime mixed layer nutrient concentrations in the North Atlantic, *Deep Sea Res., 35*, 1525–1546, 1988.

Gordon, H. R., D. K. Clark, J. W. Brown, O. B. Brown, R. H. Evans, and W. W. Broenkow, Phytoplankton pigment concentrations in the Middle Atlantic Bight: Comparison of ship determinations and CZCS estimates, *Appl. Opt., 22*, 20–36, 1983.

Hecht, M. W., F. O. Bryan, and W. R. Holland, A consideration of tracer advection schemes in a primitive equation ocean model, *J. Geophys. Res., 103*, 3301–3321, 1998.

Honjo, S., and S. J. Manganini, Particle fluxes at the interior of the northeast Atlantic (47N, 20W): A numerical simulation, *Deep Sea Res., Part II, 40*, 55–74, 1993.

Martin, J. H., S. E. Fitzwater, R. M. Gordon, C. N. Hunter, and S. J. Tanner, Iron, primary production and carbon–nitrogen flux studies during the JGOFS North Atlantic rior of the North Atlantic Ocean; studied at two JGOFS stations: 34°N 21°W and 48°N 21°W, *Deep Sea Res., Part II, 40*, 587–607, 1993.

Honjo, S., S. J. Manganini, and R. Krishfield, Cruise report: JGOFS Leg 1 International Study of the North Atlantic Bloom, *WHOI Tech. Rep. 89-22*, Woods Hole Oceanogr. Inst., Woods Hole, Mass., 1989.

Hurtt, G. C., and R. A. Armstrong, A pelagic ecosystem model calibrated with BATS data, *Deep Sea Res., Part II, 43*, 653–683, 1996.

Jenkins, W. J., Nitrate flux into the euphotic zone near Bermuda, *Nature, 331*, 521–523, 1988.

Joint, I., A. Pomroy, G. Savidge, and P. Boyd, Size-fractionated primary productivity in the northeast Atlantic in May–July 1989, *Deep Sea Res., Part II, 40*, 423–440, 1993.

Kähler, P., and W. Koeve, Marine dissolved organic matter: Can its C:N ratio explain carbon overconsumption?, *Deep Sea Res., Part I*, in press, 1999.

Koeve, W., R. W. Eppley, S. Podewski, and B. Zeitzschel, An unexpected nitrate distribution in the tropical North Atlantic at 18N, 30W – Implications for new production, *Deep Sea Res., Part II, 40*, 521–536, 1993.

Kriest, I., and G. T. Evans, Respresenting phytoplankton aggregates in biogeochemical models, *Deep Sea Res., Part I, 46*, 1841–1859, 1999.

Kupferman, S. L., G. A. Becker, W. F. Simmonst, U. Schauer, M. G. Marietta, and H. Nies, An intense cold core eddy in the northeast Atlantic, *Nature, 319*, 474–477, 1986.

Lafore, J.-P., et al., The Meso-NH atmospheric simulation system, I, Adiabatic formulation and control simulations, *Ann. Geophys., 16*, 90–109, 1998.

Lampitt, R. S., W. R. Hillier, and P. G. Challenor, Seasonal and diel variation in the open ocean concentration of marine snow aggregates, *Nature, 362*, 737–743, 1993.

Ledwell, J. R., A. J. Watson, and C. S. Law, Evidence for slow mixing across the pycnocline from an open–ocean tracer–release experiment, *Nature, 364*, 701–703, 1993.

Levitus, S., and T. Boyer, *World Ocean Atlas 1994*, vol. 4, *Temperature*, 99 pp., Natl. Environ. Satell. Data and Inf. Serv., Natl. Oceanic and Atmos. Admin., Silver Spring, Md., 1994.

Lochte, K., and O. Pfannkuche, Cyclonic cold-core eddy in the eastern Northa Atlantic, II, Nutrients, phytoplankton and bacterioplankton, *Mar. Ecol. Prog. Ser., 39*, 153–164, 1987.

Lochte, K., H. W. Ducklow, M. J. R. Fasham, and C. Stienen, Plankton succession and carbon cycling at 47°N 20°W during the JGOFS North Atlantic Bloom Experiment, *Deep Sea Res., Part II, 42*, 91–114, 1993.

Lohrenz, S. E., G. A. Knauer, V. L. Asper, M. Tuel, A. F. Michaels, and A. H. Knap, Seasonal variability in primary production and particle flux in the northwestern Sargasso Sea: US JGOFS Bermuda Atlantic Time-Series Study, *Deep Sea Res., 39*, 1373–1391, 1992.

Longhurst, A., Seasonal cycles of pelagic production and consumption, *Prog. Oceanogr., 36*, 77–167, 1995.

Marra, J., and C. Ho, Initiation of the spring bloom in the Bloom Experiment, *Deep Sea Res., Part II, 40*, 115–134, 1993.

McClain, C. R., and J. Firestone, An investigation of Ekman

upwelling in the North Atlantic, *J. Geophys. Res., 98*, 12,327–12,339, 1993.

McGillicuddy, D. J., Jr., A. R. Robinson, D. A. Siegel, H. W. Jannasch, R. Johnson, T. D. Dickey, J. McNeil, A. F. Michaels, and A. H. Knap, Influence of mesoscale eddies on new production in the Sargasso Sea, *Nature, 394*, 263–266, 1998.

Menzel, D. W., and J. H. Ryther, The annual cycle of primary production in the Sargasso Sea off Bermuda, *Deep Sea Res., 6*, 351–367, 1960.

Michaels, A. F., and A. H. Knap, Overview of the U. S. JGOFS Bermuda Atlantic Time-series Study and the Hydrostation S program, *Deep Sea Res., Part II, 43*, 157–198, 1996.

Michaels, A. F., et al., Seasonal patterns of ocean biogeochemistry at the U.S. JGOFS Bermuda Atlantic Time-series Study site, *Deep Sea Res., Part I, 41*, 1013–1038, 1994.

Michaels, A. F., D. Olson, J. L. Sarmiento, J. W. Ammerman, K. Fanning, R. Jahnke, A. H. Knap, F. Lipschultz, and J. M. Prospero, Inputs, losses and transformations of nitrogen and phosphorus in the pelagic North Atlantic Ocean, *Biogeochemistry, 35*, 181–226, 1996.

Mittelstaedt, E., Cyclonic cold-core eddy in the eastern North Atlantic. I, Physical description, *Mar. Ecol. Prog. Ser., 39*, 145–152, 1987.

Monger, B., C. McClain, and R. Murtugudde, Seasonal phytoplankton dynamics in the eastern tropical Atlantic, *J. Geophys. Res., 102*, 12,389–12,411, 1997.

Morel, A., Process studies in eutrophic, mesotrophic, and oligotrophic oceanic regimes within the tropical northeast Atlantic, in *The Changing Ocean Carbon Cycle, IGBP Book Ser.*, edited by R. B. Hanson, H. W. Ducklow, and J. G. Field, Cambridge Univ. Press, New York, pp. 338–374, 1999.

Oschlies, A., and V. Garçon, Eddy-induced enhancement of primary production in a model of the North Atlantic Ocean, *Nature, 394*, 266–269, 1998.

Oschlies, A., and V. Garçon, An eddy-permitting coupled physical-biological model of the North Atlantic, 1, Sensitivity to physics and numerics, *Global Biogeochem. Cycles, 13*, 135–160, 1999.

Oschlies, A., and J. Willebrand, Assimilation of Geosat altimeter data into an eddy-resolving primitive equation model of the North Atlantic Ocean, *J. Geophys. Res., 101*, 14,175–14,190, 1996.

Pacanowski, R., K. Dixon, and A. Rosati, The G.F.D.L Modular Ocean Model users guide version 1, *Tech. Rep. 2*, GFDL Ocean Group, Geophys. Fluid Dyn. Lab., Princeton, N. J., 1991.

Pfannkuche, O., Benthic response to the sedimentation of particulate organic matter at the BIOTRANS station, 47°N, 20°W, *Deep Sea Res., Part II, 42*, 135–149, 1993.

Robinson, M. K., R. A. Bauer, and E. H. Schroeder, Atlas of North Atlantic–Indian Ocean monthly mean temperatures and mean salinities of the surface layer, *Rep. NOO RP-18*, Nav. Oceanogr. Off., Washington, D. C., 1979.

Roman, M. R., D. A. Caron, P. Kremer, E. J. Lessard, L. P. Madin, T. C. Malone, J. M. Napp, E. R. Peele, and M. J. Youngbluth, Spatial and temporal changes in the partitioning of organic carbon in the plankton community of the Sargasso Sea off Bermuda, *Deep Sea Res., Part I, 42*, 973–992, 1995.

Sarmiento, J. L., R. D. Slater, M. J. R. Fasham, H. W. Ducklow, J. R. Toggweiler, and G. T. Evans, A seasonal three-dimensional ecosystem model of nitrogen cycling in the North Atlantic euphotic zone, *Global Biogeochem. Cycles, 7*, 417–450, 1993.

Sathyendranath, S., and A. Morel, Light emerging from the sea – Interpretations and uses in remote sensing, in *Remote Sensing Applications in Marine Science and Technology.* edited by A. P. Cracknell, pp. 232–357, D. Reidel, Norwell, Mass., 1983.

Siegel, D. A., and W. G. Deuser, Trajectories of sinking particles in the Sargasso Sea: modeling of statistical funnels above deep-ocean sediment traps, *Deep Sea Res., Part II, 44*, 1519–1541, 1997.

Siegel, D. A., D. J. McGillicuddy, and E. A. Fields, Mesoscale eddies, satellite altimetry, and new production in the Sargasso Sea, *J. Geophys. Res., 104*, 13359–13379, 1999.

Sieracki, M. E., P. G. Verity, and D. K. Stoecker, Plankton community response to sequential silicate and nitrate depletion during the 1989 North Atlantic spring bloom, *Deep Sea Res., Part II, 40*, 213–225, 1993.

Six, K. D., and E. Maier-Reimer, Effects of plankton dynamics on seasonal carbon fluxes in an ocean general circulation model, *Global Biogeochem. Cycles, 10*, 559–583, 1996.

Stammer, D., and C. W. Böning, Mesoscale varibility in the Atlantic Ocean from GEOSAT Altimetry and WOCE high resolution numerical modeling, *J. Phys. Oceanogr., 22*, 732-752, 1992.

Stammer, D., R. Tokmakian, A. Semtner, and C. Wunsch, How well does a 1/4° global circulation model simulate large-scale oceanic observation?, *J. Geophys. Res., 101*, 25,779–25,794, 1996.

Sverdrup, H. U., On the conditions for the vernal blooming of phytoplankton, *Cons. Perm. Int. Explor. Mer., 18*, 287–295, 1953.

Veldhuis, M. J. W., G. W. Kraay, and W. W. C. Gieskes, Growth and fluoroscence characteristics of ultraplankton on a north-south transect in the eastern North Atlantic, *Deep Sea Res., Part II, 40*, 609–626, 1993.

Verity, P. G., D. K. Stoecker, M. E. Sieracki, and J. R. Nelson, Grazing, growth and mortality of microzooplankton during the 1989 North Atlantic spring bloom at 47°N, 18°W, *Deep Sea Res., Part I, 40*, 1793–1814, 1993.

Veronis, G., The role of models in tracer studies, in *Numerical Models of the Ocean Circulation*, pp. 133–146, Nat. Acad. of Sci., Washington, D. C., 1975.

Weeks, A., et al., The physical and chemical environment and changes in community structure associated with bloom evolution: The Joint Global Flux Study North Atlantic Bloom Experiment, *Deep Sea Res., Part II, 40*, 347–368, 1993.

Yoder, J. A., C. R. McClain, and G. C. Feldman, Annual cycles of phytoplankton chlorophyll concentrations in the global ocean: A satellite view, *Global Biogeochem. Cycles, 7*, 181–193, 1993.

Zenk, W., B. Klein, and M. Schröder, Cape Verde Frontal Zone, *Deep Sea Res., Part I, 38*, suppl., 505–530, 1991.

V. Garçon, Centre National de la Recherche Scientifique, UMR5566/LEGOS, 18 Avenue Edouard Belin, 31401 Toulouse Cedex 4, France. (garcon@pontos.cst.cnes.fr)

W. Koeve and A. Oschlies, Institut für Meereskunde an der Universität Kiel, Düsternbrooker Weg 20, 24105 Kiel, Germany. (wkoeve@ifm.uni-kiel.de), (aoschlies@ifm.uni-kiel.de)

(Received June 4, 1999; revised August 25, 1999; accepted September 2, 1999.)